Constraints on particle properties from the cosmic microwave background

Dissertation

submitted to the

Faculty of Physics,

Bielefeld University

by

Isabel Mira Oldengott

June 2017

Supervisor: Prof. Dr. Dominik J. Schwarz

Für Jan.

List of publications

As part of this dissertation the following publications have been published:

1. **JCAP 1608 (2016) no. 08, 054** (chapter 4)

   I. M. Oldengott, D. Boriero, and D. J. Schwarz, "Reionization and dark matter decay," JCAP 1608 (2016) no. 08, 054, arXiv:1605.03928 [astro-ph.CO].

   http://dx.doi.org/10.1088/1475-7516/2016/08/054

2. **JCAP 1504 (2015) no. 04, 016** (chapter 5.1)

   I. M. Oldengott, C. Rampf, and Y. Y. Y. Wong, "Boltzmann hierarchy for interacting neutrinos I: formalism," JCAP 1504 (2015) no. 04, 016, arXiv:1409.1577 [astro-ph.CO].

   http://dx.doi.org/10.1088/1475-7516/2015/04/016

3. **JCAP 1711 (2017) no. 11, 027** (chapter 5.2)

   I. M. Oldengott, T. Tram, C. Rampf, and Y. Y. Y. Wong, "Interacting neutrinos in cosmology: Exact description and constraints," JCAP 1711 (2017) no. 11, 027, arXiv:1706.02123 [astro-ph.CO].

   http://dx.doi.org/10.1088/1475-7516/2017/11/027

4. **Europhys. Lett. 119 (2017) no. 2, 29001** (chapter 6)

   I. M. Oldengott and D. J. Schwarz, "Improved constraints on lepton asymmetry from the cosmic microwave background," Europhys. Lett. 119 (2017) no. 2, 29001, arXiv:1706.01705 [astro-ph.CO].

   http://dx.doi.org/10.1209/0295-5075/119/29001

Abstract

In this thesis, we derive constraints on various particle properties from observations of the cosmic microwave background (CMB).

In our first project [1], we consider a decaying dark matter component as a source of reionization in addition to the reionization process caused by astrophysical objects. Both of these reionization sources impact the angular power spectrum of the CMB in a similar way. We take into account two different parametrizations for the astrophysical reionization process. Using Planck 2015 data, we constrain the effective dark matter decay rate to $\Gamma_{\rm eff} < 2.9 \times 10^{-25}/\mathrm{s}$ at 95% CL. This limit is robust, as it only weakly depends on the chosen parametrization of astrophysical reionization. We also apply our results to a keV-mass sterile neutrino as a specific dark matter candidate and obtain constraints on its mixing angle and mass.

In a second project [2,3], we study and constrain the impact of non-standard neutrino interactions on the CMB angular power spectrum. In the first part of this project [2], we derive the Boltzmann hierarchy for neutrinos including interactions with a scalar particle. We study two limits of the scalar mass, an extremely massive scalar that only plays the role of a mediator for neutrino self-interactions, and a massless scalar that can be produced in abundance and demands its own Boltzmann hierarchy. In contrast to the Boltzmann hierarchy for photons, our interacting neutrino/scalar Boltzmann hierarchies are momentum dependent, which reflects non-negligible energy transfer in the considered neutrino interactions. In the second part of this project [3], we focus on the massive scalar case and implement the Boltzmann hierarchy for interacting neutrinos (derived in [2]) into the Boltzmann solver CLASS. We compare our results with known approximations in the literature, finding thereby a good agreement between our exact approach and the relaxation time approximation (RTA). The popular $\left(c^2_{\rm eff}, c^2_{\rm vis}\right)$-parametrization however does not reproduce the correct signal in the CMB angular power spectrum. Using the RTA, we furthermore derive constraints on the effective coupling constant $G_{\rm eff}$ from currently available cosmological data. Our results reveal a bimodal posterior distribution, where one mode represents the standard ΛCDM limit, and the other a scenario of neutrinos self-interacting with $G_{\rm eff} \simeq 3 \times 10^9\, G_{\rm F}$.

In a third project [4], we consider a cosmic lepton asymmetry $\eta_{\rm l}$, which affects the CMB angular power spectrum through a modified helium abundance and an increased expansion rate in the early Universe. We derive constraints on the neutrino chemical potentials from the Planck 2015 data and find $\xi = -0.002^{+0.114}_{-0.111}$ (95% CL) for the chemical potentials, corresponding to $-0.085 \leq \eta_{\rm l} \leq 0.084$. Our constraints on the lepton asymmetry are significantly stronger than previous constraints from CMB data analysis and more robust than those from primordial light element abundances.

Contents

1 Introduction

Cosmology deals with the evolution of the Universe as a whole. It therefore naturally needs input from a variety of other physical disciplines: Energy and matter are embedded into a space time that is described by general relativity (or modified gravity). Kinetic theory is applied in order to follow the evolution of different particle densities in an expanding Universe. The description of the hot and dense early Universe – in which matter was broken down into its basic constituents – needs input from particle physics. The formation of the first light nuclei is in contrast described by nuclear physics and the formation of the cosmic microwave background (CMB), caused by the formation of neutral atoms, is based on atomic physics. Astrophysical input is important to describe the epoch of reionization and basically whenever it comes to cosmological observations.

On the other hand, cosmology can also provide interesting insights into all of those research fields. Whereas the impact of cosmological observations on theories like nuclear or atomic physics is certainly rather limited, the potential of cosmology to constrain particle physics and particularly physics beyond the Standard Model (SM) is remarkable. In this thesis, we derive constraints on different particle properties from observations of the cosmic microwave background, using data from the Planck satellite [5]. We thereby focus on two elusive components of our Universe: dark matter and neutrinos.

The term "dark matter (DM)" refers in general to the phenomenon that various cosmological and astrophysical observations cannot be explained by the amount of observed matter and our gravity theory alone. Possible solutions to this apparent contradiction encompass theories of modified gravity as well as the existence of non-standard particles which only interact via gravity and possibly via the weak force. We only consider the second possibility in this thesis, i.e. dark matter in form of one or several particle species. In chapter 4, we consider a dark matter component that decays into electromagnetically interacting daughter particles. These daughter particles can contribute as an additional source to the conventional reionization process by astrophysical objects. We derive constraints on the dark matter decay rate from observations of the CMB temperature and polarization anisotropy spectrum. Possible candidates for decaying dark matter are numerous in theories of physics beyond the SM. We however apply our results specifically to the case of a sterile neutrino with a mass in the

keV-range. This work was published in [1].

Another elusive particle component of our Universe are SM neutrinos. Whereas the existence of dark matter *in form of particles* may be favoured by most physicists (but still arguable), the existence of active neutrinos is indisputable. The nature of neutrinos however remains one of the last remaining puzzles of the SM of particles physics. The SM explicitly assumes massless neutrinos, which is in contradiction to the observation of neutrino oscillations. Any attempt to add neutrino masses necessitates new physics. Properties like the masses of neutrinos, their nature (Dirac or Majorana fermions) and to some extent also their interaction properties are still unknown. In chapter 5, we consider the possibility that neutrinos have additional, non-standard interactions with a scalar particle via Yukawa-coupling. In section 5.1 we derive the Boltzmann hierarchy of interacting neutrinos for the case of a very massive scalar particle (where the new interaction is effectively Fermi-like) as well as for the case of a massless scalar particle. Based on this Boltzmann hierarchy, we study the impact of interacting neutrinos on the CMB in section 5.2. We thereby focus on the case of a massive scalar and furthermore derive constraints on the neutrino–scalar coupling. The work presented in chapter 5 was published in the publications [2] and [3].

In chapter 6, we derive constraints on another parameter related to neutrino physics, namely lepton asymmetry. A lepton asymmetry – possibly large than the baryon asymmetry by orders of magnitude – could be hidden in the cosmic neutrino background and leads to modifications of big bang nucleosynthesis (BBN) and the CMB. This work was published in [4].

The rest of this thesis is structured as follows: In the next three sections we give a short introduction to the basics of our standard cosmological theory. In chapter 2 we summarize the theory and results of BBN. We furthermore study the impact of an additional isotope, namely ^{6}He, on the outcome of BBN. An introduction to the theory of the CMB is given in chapter 3, including a summary of recombination and cosmic perturbation theory. After the presentation of the main results in chapters 4, 5 and 6 we conclude in chapter 7.

1.1 Basic cosmology

The cosmological standard model assumes that our Universe is expanding, starting its evolution from an initially hot an dense state. This idea rests on three pillars: the Hubble diagram, the formation of light nuclei in the early Universe and the cosmic microwave background. The last two of them are described in chapters 2 and 3. Let us begin this section with explaining the first one, i.e. the Hubble law. The physics

described in this and the following section 1.2 can be found in standard cosmology text books like [6–10] Throughout this work we use natural units, i.e. $k_{\rm B} = \hbar = c = 1$.

In 1929 Edwin Hubble observed that the more distant galaxies are located to us the faster they move away from us (Hubble law) [11]. The *cosmological principle* furthermore states that our Universe is isotropic and homogeneous at large scales ($\gtrsim 100$ Mpc). An expanding, homogeneous and isotropic Universe can be described by the Friedmann-Lemaître-Robertson-Walker (FLRW) metric,

$$\mathrm{d}s^2 = g_{\mu\nu}\mathrm{d}x^\mu \mathrm{d}x^\nu = -\mathrm{d}t^2 + a^2(t)\left(\frac{\mathrm{d}r^2}{1-kr^2} + r^2(\mathrm{d}\theta^2 + \sin^2\theta \mathrm{d}\phi^2)\right), \tag{1.1}$$

where a (as a function of cosmic time) is the scale factor that describes the expansion of the Universe. The parameter k describes the curvature of space which can be positive, negative or flat ($k = 0$). In most of this work, we consider a flat Universe in which the FLRW metric can be written in Cartesian coordinates,

$$\mathrm{d}s^2 = -\mathrm{d}t^2 + a^2(t)\left(\mathrm{d}x^2 + \mathrm{d}y^2 + \mathrm{d}z^2\right). \tag{1.2}$$

The FLRW metric (1.1) is also often rewritten in terms of conformal time $\mathrm{d}\tau = a^{-1}\mathrm{d}t$.

The FLRW space time also allows us to the recover the Hubble law: Physical distances are given by $d = a(t)r$, where r denotes coordinate distances, $r = \sqrt{\delta_{ij}\Delta x^i \Delta x^j}$. The velocity of galaxies with respect to us is then simply given by (assuming no peculiar velocity)

$$v = \dot{d} = \dot{a}r = Hd, \tag{1.3}$$

where we defined the Hubble rate as

$$H(t) \equiv \frac{\dot{a}(t)}{a(t)}. \tag{1.4}$$

For relatively nearby galaxies the Hubble rate can be evaluated today, i.e. $H(t) = H_0$. The *Hubble constant* is often also written as

$$H_0 = h \cdot 100 \frac{\mathrm{km}}{\mathrm{s}\cdot\mathrm{Mpc}}. \tag{1.5}$$

The velocities of nearby galaxies are therefore approximately proportional to their physical distances, with a proportionality constant of H_0. To measure the distance of a galaxy requires however the appearance of *standard rulers*, i.e. objects of known luminosity. In figure 1.1, we show a Hubble diagram (i.e. a velocity-versus-distance diagram) from the Hubble Space Telescope [12], where Cepheids have been used as standard candles to measure the galaxy distances.

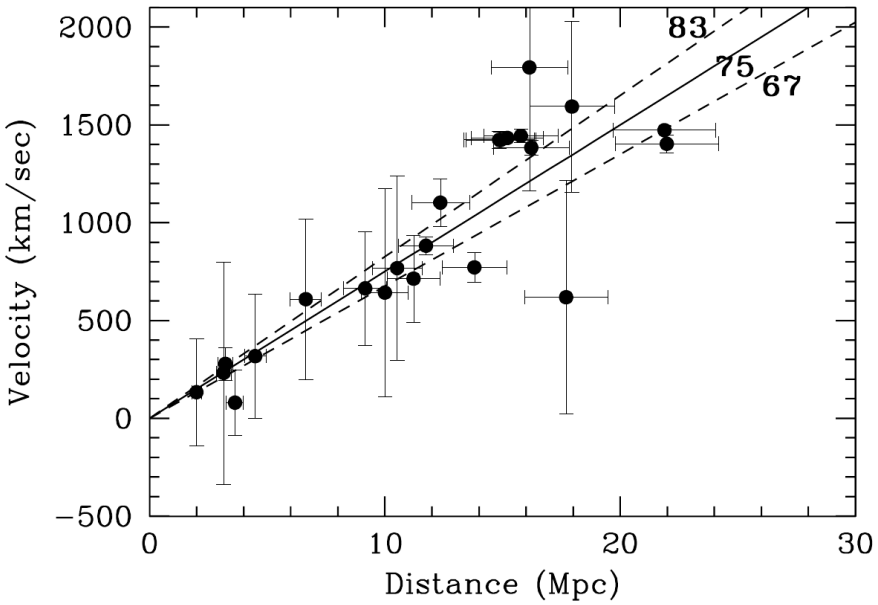

Figure 1.1: Hubble Diagram (velocity versus distance) for galaxies with Cepheid distances, measured by the Hubble Space Telescope [12].

By applying the FLRW metric to the geodesic equation we furthermore find that the wavelength of light gets stretched due to the expansion of space, $\lambda \propto a$. The same also holds for the physical momenta of massive particles. This motivates the introduction of the concept of *cosmological redshift*,

$$1 + z \equiv \frac{a_0}{a}, \tag{1.6}$$

where a_0 is the scale factor today. By rescaling r in the FLRW metric (1.1), usually either a_0 is set to 1 or the curvature parameter is reduced to the values $k = 0, \pm 1$.

Applying the FLRW metric (1.1) to the Einstein equation (time–time component) gives the first Friedmann equation,

$$H^2(t) = \frac{\dot{a}^2}{a^2} = \frac{8\pi G}{3}\rho + \frac{\Lambda}{3} - \frac{k}{a^2}. \tag{1.7}$$

Here, we assumed the energy-momentum tensor to be that of a perfect fluid, i.e. $T^{\mu}{}_{\nu} = \mathrm{diag}(-\rho, \mathcal{P}, \mathcal{P}, \mathcal{P})$, where ρ denotes the sum of the energy densities and $\mathcal{P}$ the sum of the pressures of all particle species in the Universe. Λ is the cosmological constant, which can be interpreted either as a geometrical property (writing it on the l.h.s. of the Einstein equation) or as some form of vacuum energy (writing it on the r.h.s. of the Einstein equation as a part of the energy-momentum tensor). The latter interpretation

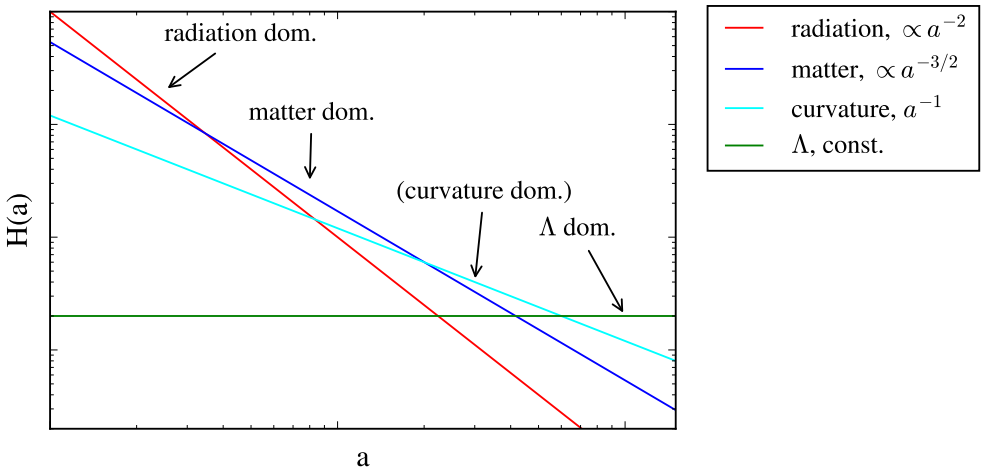

Figure 1.2: Illustration of the logarithmic dependence of the Hubble expansion rate on the scale factor, dominated by different components of the Universe (in arbitrary units).

implies $\mathcal{P}_\Lambda = -\rho_\Lambda$.

In addition to the Friedmann equation we obtain another equation by the local covariant conservation of the energy-momentum tensor (continuity equation),

$$\begin{aligned} \nabla_\mu T^\mu{}_\nu = 0 \;&\Rightarrow\; \dot{\rho} + 3\frac{\dot{a}}{a}(\rho + \mathcal{P}) = 0 \\ &\Rightarrow\; \frac{\dot{\rho}}{\rho} = -3(1+w)\frac{\dot{a}}{a}, \end{aligned} \tag{1.8}$$

where we introduced the equation of state by $\mathcal{P} \equiv w\rho$. The values of the equation of state for some relevant cases can be found in table 1.1. Note that the continuity equation (1.8) holds always for the sum of all particle species, but it also holds for individual components as long as they are in equilibrium. Assuming a constant equation of state the solution of equation (1.8) is given by

$$\rho_i \propto a^{-3(1+w_i)}. \tag{1.9}$$

It is convenient to use this result (1.9) and rewrite the Friedmann equation as ($a_0 = 1$)

$$H(a) = H_0 \left(\Omega_\mathrm{R} a^{-4} + \Omega_\mathrm{M} a^{-3} + \Omega_\mathrm{k} a^{-2} + \Omega_\Lambda\right)^{1/2}, \tag{1.10}$$

with

$$\Omega_\mathrm{R} = \frac{\rho_{\mathrm{R},0}}{\rho_{\mathrm{cr},0}}, \quad \Omega_\mathrm{M} = \frac{\rho_{\mathrm{M},0}}{\rho_{\mathrm{cr},0}}, \quad \Omega_\Lambda = \frac{\rho_{\Lambda,0}}{\rho_{\mathrm{cr},0}}, \quad \Omega_\mathrm{k} = -\frac{k}{H_0^2} \quad \text{and} \quad \rho_{\mathrm{cr},0} = \frac{3H_0^2}{8\pi G}. \tag{1.11}$$

dominant contribution	w	$\rho(a)$	$H(a)$	$a(t)$	$H(t)$
matter	0	$\propto a^{-3}$	$\propto a^{-3/2}$	$\propto t^{2/3}$	t^{-1}
radiation	$\frac{1}{3}$	$\propto a^{-4}$	$\propto a^{-2}$	$\propto t^{1/2}$	t^{-1}
Λ	-1	const.	const.	$\propto e^{Ht}$	const.
negative k			a^{-1}	$\propto t$	t^{-1}

Table 1.1: Solutions of the Friedmann equation (1.7) and the continuity equation (1.8), for the different components of the Universe.

We find by definition that $\Omega_{\mathrm{R}} + \Omega_{\mathrm{M}} + \Omega_{\mathrm{k}} + \Omega_{\Lambda} = 1$. From equation (1.10) we see that the expansion of the Universe must be dominated by different components at different times, see figure 1.2. Of course, whether the Universe was or ever will be dominated by a certain component depends also on the values of Ω_i realized in nature. We will discuss this in more detail in 1.3

In order to furthermore find the time dependence of the scale factor $a(t)$ we have to simultaneously solve equation (1.7) and (1.8). In general, for a mixture of different particle species (relativistic and non-relativistic) and in the presence of a cosmological constant and a curvature term this has to be done numerically. However, in case of a single contribution we can find simple analytical solutions for $a(t)$,

$$a(t) \propto \begin{cases} t^{\frac{2}{3(1+w)}}, & w \neq -1 \\ e^{Ht}, & w = -1 \\ t, & \text{negative } k. \end{cases} \tag{1.12}$$

Equation (1.12) holds exactly if only a single component exists, and approximately if one component is dominating the evolution of the Hubble expansion rate. The analytical solutions are summarized in table 1.1. Note that the case of negative curvature domination (Milne Universe) has by definition no source of energy density and therefore there exists no equation of state. Positive curvature can never be the only source term on the right hand side of the Friedmann equation (1.7), as this would induce an imaginary scale factor. However, whereas all cases presented in table 1.1 lead to eternal expansion, inclusion of positive curvature can result in a turning point of the expansion of the Universe, followed by a contracting phase that ends in a *big crunch*.

1.2 Kinetic theory in an expanding Universe

The Friedmann equation (1.7) and the continuity equation (1.8) describe the evolution of the scale factor and the energy density of a *single* fluid containing *all* particles. If each individual particle species would always remain in equilibrium, the evolution of

the individual energy densities would entirely be described by individual continuity equations and their macroscopic quantities would follow the laws of thermodynamics. However, due to the expansion of space, the different particle species drop out of equilibrium (decoupling or freeze-out) or eventually enter equilibrium (recoupling or freeze-in) at some point. The evolution of the individual particle species must therefore be described within the framework of kinetic theory, which is described in more detail in textbooks like [6,7,13].

Our starting point is the relativistic Boltzmann equation [1],

$$\mathcal{L}(f) = \mathcal{C}(f). \tag{1.13}$$

The left hand side is the Liouville operator acting on the single-particle phase space distribution f,

$$\mathcal{L}(f) \equiv \frac{\mathrm{d}f}{\mathrm{d}t}\left(x^\mu, P^\mu\right) \tag{1.14}$$

where the four-momentum P^μ is defined as

$$P^\mu = mu^\mu = m\frac{\mathrm{d}x^\mu}{\mathrm{d}\lambda}. \tag{1.15}$$

The right hand side is the collision integral that takes into account binary particle collisions. Macroscopic quantities like number density, energy density and pressure are given by momentum integrals over the phase space distribution.

Let us first focus on the case with no particle interactions, i.e. $\mathcal{C}(f) = 0$. In this case, the collisionless Boltzmann equation can be rewritten as

$$\begin{aligned}\mathcal{L}(f) =& \frac{m}{P^0}\left[\frac{\mathrm{d}f}{\mathrm{d}\lambda}\left(x^\mu, P^\mu\right)\right] = \frac{m}{P^0}\left[\frac{\partial f}{\partial x^\mu}\frac{\mathrm{d}x^\mu}{\mathrm{d}\lambda} + \frac{\partial f}{\partial P^\nu}\frac{\mathrm{d}P^\nu}{\mathrm{d}\lambda}\right] \\ =& \frac{1}{P^0}\left[\frac{\partial f}{\partial x^\mu}P^\mu - \frac{\partial f}{\partial P^\nu}\Gamma^\nu_{\rho\sigma}P^\rho P^\sigma\right] = 0,\end{aligned} \tag{1.16}$$

where λ is an affine parameter. $\Gamma^\nu_{\rho\sigma}$ denote the Christoffel symbols that were introduced into equation (1.16) by using the geodesic equation,

$$\frac{\mathrm{d}u^\nu}{\mathrm{d}\lambda} + \Gamma^\nu_{\rho\sigma}u^\rho u^\sigma = 0. \tag{1.17}$$

[1] Let us briefly mention here that the more fundamental equation is the N-particle Liouville equation that acts on the N-particle phase space distribution, e.g. [14]. An equivalent formulation to this N-particle Liouville equation is the BBGKY hierarchy which is a coupled system of N differential equations for the *reduced* phase-space densities. The BBGKY hierarchy can be reduced to the Boltzmann equation (1.13) by applying the *Boltzmann Stoßzahlansatz*, which states that the velocities of particles are entirely uncorrelated before scattering. In this case, the two-particle phase space density is simply a product of single-particle phase space distributions. The Boltzmann equation is therefore strictly speaking only valid for dilute gases, for which the inter-particle distance is much larger than the interaction range.

In a homogeneous and isotropic Universe the single-particle phase space density f only depends on time t and $P = \sqrt{\delta_{ij} P^i P^j}$ (or equivalently P^0 by using the mass-shell condition), but is independent of x^i and the direction of P^i. Hence, after inserting the Christoffel symbols of a flat FLRW metric (1.2) into the Liouville operator (1.16) we find

$$\mathcal{L}(f) = \left(\frac{\partial f(P,t)}{\partial t} - 2HP \frac{\partial f(P,t)}{\partial P} \right) = 0. \tag{1.18}$$

This equation is satisfied by any arbitrary function of $(a^2 P)$.

It is however physically more intuitive to rewrite the Liouville equation in terms of the *physical* momentum p^i, i.e. the momentum measured by an observer in the rest frame of the FLRW metric (1.2). Such a resting observer is described by $u^\mu_{\text{obs}} = (1,0,0,0)$ and the measured energy is simply $E = g_{\mu\nu} P^\mu u^\nu_{\text{obs}} = P^0$. The physical momentum is therefore given by

$$\begin{aligned} p^2 = \delta_{ij} p^i p^j = E^2 - m^2 = E^2 + P_\mu P^\mu = a^2 P^2 = a^2 \delta_{ij} P^i P^j \\ \Rightarrow P^i = \frac{1}{a} p^i. \end{aligned} \tag{1.19}$$

We can now rewrite equation (1.18) in terms of the physical momentum as

$$\mathcal{L}(f) = \left(\frac{\partial f(p,t)}{\partial t} - Hp \frac{\partial f(p,t)}{\partial p} \right) = 0. \tag{1.20}$$

As already mentioned in the previous section, physical momenta experience redshift due to the expansion of space. By introducing yet another momentum, the comoving momentum $q = ap$, we can separate out the effect due to expansion and the Liouville equation simplifies further to

$$\frac{\partial f(q,t)}{\partial t} = 0. \tag{1.21}$$

Let us now study the case of particle scattering. The collision term on the r.h.s. of equation (1.13) for binary collisions ($a + b \to c + d$) in terms of physical momentum p is given by (e.g. [7])

$$\begin{aligned} \mathcal{C}[f_a(p_a,t)] = & \frac{1}{E_a} \int \mathrm{d}\pi(p_b)\, \mathrm{d}\pi(p_c)\, \mathrm{d}\pi(p_d) (2\pi)^4 \delta^{(4)}(p_a + p_b - p_c - p_d) \\ & \times |\mathcal{M}_{ab\to cd}|^2 \left[f_c(p_c,t) f_d(p_d,t) \left(1 \pm f_a(p_a,t)\right) \left(1 \pm f_b(p_b,t)\right) \right. \\ & \left. - f_a(p_a,t) f_b(p_b,t) \left(1 \pm f_c(p_c,t)\right) \left(1 \pm f_d(p_d,t)\right) \right], \end{aligned} \tag{1.22}$$

with

$$\mathrm{d}\pi(p) = \frac{\mathrm{d}^3 p}{(2\pi)^3 2E(p)}. \tag{1.23}$$

The second line in (1.22) is a gain term, i.e. it takes into account the particles that are scattered into the considered phase space volume element, whereas the third line is a loss term taking into account the particles scattered out of it. Note that we explicitly assumed invariance under time reversal by setting $|\mathcal{M}_{ab\to cd}|^2 = |\mathcal{M}_{cd\to ab}|^2$ for the squared scattering amplitude. The $(1 \pm f)$-terms take into account the effect of Pauli-blocking for fermions (minus) and Bose enhancement for bosons (plus).

As mentioned before, number density n, energy density ρ and pressure P are obtained by momentum integration of the phase space distribution, i.e. [2]

$$\begin{aligned} n &= \int \frac{\mathrm{d}^3p}{(2\pi)^3} f(p,t), \\ \rho &= \int \frac{\mathrm{d}^3p}{(2\pi)^3} E f(p,t), \\ P &= \frac{1}{3}\int \frac{\mathrm{d}^3p}{(2\pi)^3} \frac{p^2}{E} f(p,t). \end{aligned} \tag{1.24}$$

By integrating the Boltzmann equation over momentum respectively, we therefore obtain equations describing the time evolution of n, ρ and P. For the case of elastic scattering events ($a + b \to a + b$) number and energy of particle species a and b are conserved and we expect the *integrated* collision integral $\mathcal{C}$ to vanish. Indeed, this can be shown explicitly by basic symmetries of the collision integral, see e.g. [13].

Noteworthy, the *un-integrated* collision integral $\mathcal{C}[f]$ vanishes in two drastically different situations, i.e. when particles are in equilibrium or when they are not interacting at all. We can distinguish between two different forms of equilibrium: *Kinetic equilibrium* holds when elastic scattering events ($a+b \to a+b$) are in equilibrium and *chemical equilibrium* holds when furthermore number changing processes ($a+b \to c+d$) are in equilibrium. For massless particles, the equilibrium distribution is simply a Fermi-Dirac or Bose-Einstein distribution, where all particles share the same temperature (kinetic equilibrium) and the chemical potentials fulfil (chemical equilibrium)

$$\mu_a + \mu_b = \mu_c + \mu_d. \tag{1.25}$$

Inserting the Fermi-Dirac/Bose-Einstein distribution of massless particles into the Liouville operator (1.20) furthermore reveals that

$$\frac{1}{T} \propto a \qquad \text{and} \qquad \frac{\mu}{T} = \text{const.} \tag{1.26}$$

in order to fulfil $\mathcal{L}(f) = 0$.

[2] Depending on the normalization of f, different prefactors in (1.24) may appear. We follow here the notation of [13].

An intriguing fact is that massive particles in contrast are strictly speaking never in equilibrium in an expanding space time [13]. A massive Fermi-Dirac or Bose-Einstein distribution fulfils $\mathcal{C}[f] = 0$, but not $\mathcal{L}[f] = 0$ at the same time. For sufficiently slow expansion rates (1.2) or for sufficiently high interaction rates, equilibrium is however nearly realized.

Out of equilibrium we have $C[f] \neq 0$, and there are in general no trivial solutions to the Boltzmann equation (1.13). As a non-linear integro-differential equation, the Boltzmann equation must be solved numerically in general. It is however the most powerful tool in order to study non-equilibrium physics and has many applications in the cosmological standard model and beyond.

1.3 Cosmological standard model

After having introduced the foundations of cosmology, we now come to our cosmological standard model, the so called ΛCDM model. The ΛCDM model assumes zero curvature ($k = 0$) and a cosmological constant Λ. Additionally to the particles described within the SM of particle physics it includes cold dark matter. Let us explain those different components in the following in more detail.

Zero curvature Cosmological observations show that our Universe is very close to being flat today, i.e. $\Omega_\mathrm{k} = -0.004^{+0.015}_{-0.015}$ (95% CL) [5]. Such a small value of Ω_k today seems to require an unnatural amount of fine tuning as we will see in the following. Let us first define

$$\Omega(t) \equiv \frac{8\pi G}{3H^2}\rho + \frac{\Lambda}{3H^2}. \tag{1.27}$$

From the Friedmann equation (1.7) we see that a flat Universe implies

$$\Omega(t) - 1 = \frac{k}{H^2 a^2} = 0 \qquad \Rightarrow \qquad \frac{\mathrm{d}}{\mathrm{d}t}\left(\Omega(t) - 1\right) = \frac{\mathrm{d}}{\mathrm{d}t}\left(\frac{k}{\dot{a}}\right) = -2\ddot{a}\left(\Omega(t) - 1\right). \tag{1.28}$$

During matter and radiation domination ($\ddot{a} < 0$) a flat Universe with $\Omega(t) = 1$ is therefore an unstable fixed point, i.e. it should quickly diverge and evolve curvature. A solution to this *flatness problem* can however be found if there was a period of inflationary growth of the Universe before radiation domination. This inflationary epoch is believed to be caused by one or more quantum fields, the inflaton fields. In section 3, we briefly discuss another motivation for the inflationary paradigm which relates to the uniformness of CMB. The theory of inflation has been first proposed by [15, 16] and is now part of our ΛCDM model (and the reason why curvature is explicitly assumed to be zero).

Cold dark matter As we have already mentioned in the beginning of this chapter, cosmological observations show that either our gravity theory is incomplete or most of the matter in our Universe exists in form of non-standard (maximally weakly interacting) particles. Those observations include for example the rotation curves of galaxies [17, 18], gravitational lensing [19, 20] and the CMB [5, 21]. The ΛCDM model explicitly assumes the second explanation, i.e. the existence of cold dark matter particles. The energy density of cold dark matter is measured by CMB observations [5] as $\Omega_c h^2 = 0.1193 \pm 0.0014$, whereas the amount of baryonic matter in our Universe is only $\Omega_b h^2 = 0.02226 \pm 0.00016$.

Cosmological constant The observation of type Ia supernovae reveal that the expansion of our Universe is accelerated today. This was discovered in 1998 by Supernova Cosmology Project [22] and the High-Z Supernova Search Team [23] and honoured by the Nobel Prize in 2011. This phenomenon of accelerated expansion of space is generally referred to as *dark energy*. As we saw in section 1.1, a simple explanation is provided by the existence of a cosmological constant Λ. From observations of the CMB we find $\Omega_\Lambda = 0.6879 \pm 0.0087$ [5]. Even though a cosmological constant is entirely consistent with general relativity, its appearance raises some open questions. The energy density of the cosmological constant is smaller by a factor of $\sim 10^{120}$ than the expected vacuum energy from particle physics. Furthermore, the fact that we observe $(\Omega_\Lambda, \Omega_\mathrm{m}) \approx (0.7, 0.3)$ in our Universe today raises a fine-tuning problem. See e.g. [24] for a review and discussion on the cosmological constant.

2 Big bang nucleosynthesis

In this chapter, we discuss the phenomenology of big bang nucleosynthesis. More comprehensive reviews can be found e.g. in [25, 26].

The theory of BBN describes the formation of the first nuclei in the early Universe. At early times, protons and neutrons are converted into each other by weak scattering processes

$$p + e^- \leftrightarrow n + \nu_e, \qquad p + \bar{\nu}_e \leftrightarrow n + e^+ \tag{2.1}$$

and neutron decay

$$n \leftrightarrow p + e^- + \bar{\nu}_e, \tag{2.2}$$

which keep them in kinetic and chemical equilibrium. The ratio of the neutron to proton number density in equilibrium is simply given by (at $T \ll m_\mathrm{n}$)

$$\left(\frac{n}{p}\right)_\mathrm{eq} = \frac{e^{-m_\mathrm{n}/T} \int \mathrm{d}p\, p^2 e^{-p^2/(2m_\mathrm{n}T)}}{e^{-m_\mathrm{p}/T} \int \mathrm{d}p\, p^2 e^{-p^2/(2m_\mathrm{p}T)}} \approx e^{-Q/T}, \tag{2.3}$$

where $Q = m_\mathrm{n} - m_\mathrm{p} = 1.293$ MeV [27]. At high temperatures ($T \gg Q$) neutrons and protons are therefore equally abundant, whereas the neutron-to-proton ratio (2.3) gets suppressed with decreasing temperature.

At a temperature of ~ 1 MeV weak interactions (2.1) freeze out [7], which also marks the temperature at which neutrinos decouple from the cosmic plasma. Afterwards, the neutron-to-proton ratio is only altered by neutron decay (2.2).

Naively one may expect that the production of deuterium already starts as soon as the temperature drops beneath the binding energy of deuterium (~ 2.2 MeV). But due to the high photon-to-baryon ratio, high energetic photons from the tail of the photon distribution destroy any newly formed deuterium instantaneously. Therefore, the onset of big bang nucleosynthesis is delayed until $T \sim 0.1$ MeV. At this time, the neutron-to-proton ratio has decreased by neutron decay to $(n/p)_\mathrm{BBN} \sim 1/7$ [26].

In standard BBN, the primordial abundance of nuclei depends on only one free parameter, the baryon-to-photon ratio η. This parameter is related to the baryon density

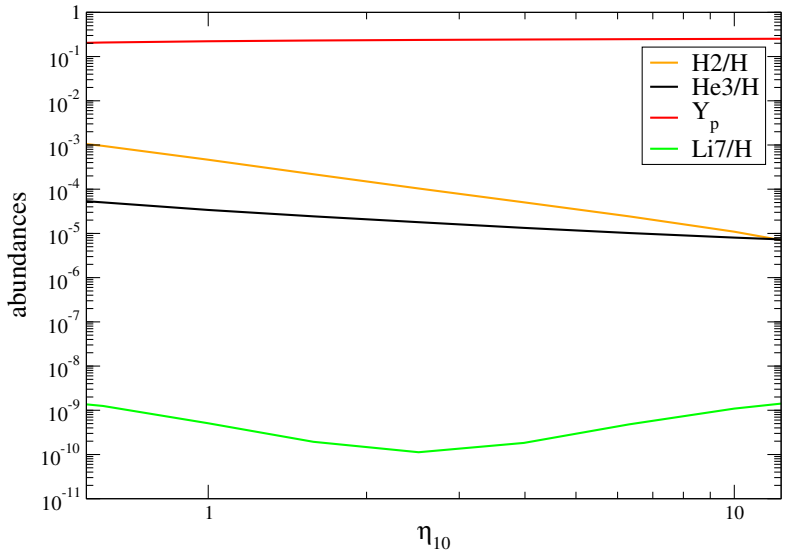

Figure 2.1: Primordial abundances of ^{4}He (red), D (orange), ^{3}He (black) and ^{7}Li (green) as a function of η_{10}, (computed with the Kawano Code [29]).

$\Omega_b h^2$ (after electron-positron annihilation) according to [28]

$$\eta_{10} \equiv 10^{10}\eta \equiv 10^{10}\frac{n_b - n_{\bar{b}}}{n_\gamma} \approx 274\,\Omega_b h^2. \tag{2.4}$$

.

Figure 2.1 shows the dependence of the primordial abundance of ^{4}He, D, ^{3}He and ^{7}Li on η_{10}. The general trends of figure 2.1 are relatively easy to understand: Since there is a local maximum in the nuclear binding energy at nucleon number 4 and there are no stable nuclei with nucleon number 5, the abundance of elements heavier than ^{4}He is strongly suppressed. Nearly all of the available neutrons are rapidly burned into ^{4}He, whose abundance is therefore limited by the neutron-to-proton ratio at the onset of BBN. The mass fraction of ^{4}He can immediately be estimated as

$$Y_p \equiv \frac{m_{He}N_{He}}{m_{He}N_{He} + m_H N_H} \approx \frac{4N_{He}}{4N_{He} + N_H} \approx \frac{2(n/p)_{BBN}}{1 + (n/p)_{BBN}} \approx 0.25, \tag{2.5}$$

where we used $N_{He} \approx N_n/2$ and $N_H \approx N_p - 2N_{He} \approx N_p - N_n$. This simple and remarkably good estimate also helps us to understand the dependency of Y_p on η_{10}: A higher η_{10} causes BBN to start earlier, which in turn leads to a larger neutron-to-proton ratio at the onset of BBN, $(n/p)_{BBN}$. Since ^{4}He is mainly determined by the available neutrons (2.5), the ^{4}He abundance increases with η_{10}.

Furthermore, a high baryon density implies a high nucleon density and D and ^{3}He are burned faster into ^{4}He. The final abundances of D and ^{3}He therefore decrease with

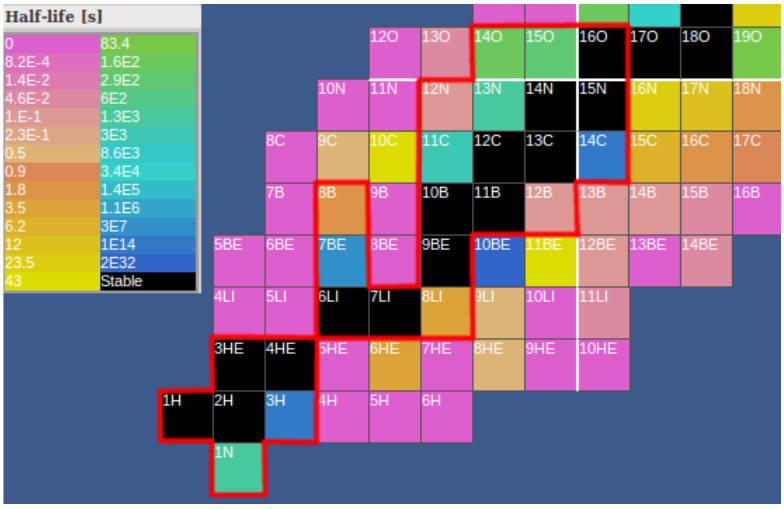

Figure 2.2: Cut from the nuclide chart, nuclides framed in red are those considered in the PArthENoPE code, (credit: www-nds.iaea.org).

η_{10}. Since D has the strongest dependency on η_{10}, it is considered to be a good *baryometer*, i.e. it has the highest potential to give a precise measurement of η_{10}.

The shape of the ^{7}Li curve in figure 2.1 is more complicated, as it reflects two different production paths: For low baryon density the dominant channel to produce ^{7}Li is the direct production via $^3\mathrm{H}+\alpha \rightarrow {}^7\mathrm{Li}+\gamma$. Since ^{7}Li is easily destroyed by protons via $^7\mathrm{Li} + \mathrm{p} \rightarrow {}^4\mathrm{He} + {}^4\mathrm{He}$, its abundance decreases with increasing η_{10}. For higher nucleon densities, ^{7}Li is instead mainly produced by the electron capture of ^{7}Be at much later times, when protons are cool enough to not destroy ^{7}Li any longer. Due to its higher charge ^{7}Be is harder to destroy by protons than ^{7}Li. Therefore, an increased baryon density simply leaves more time to produce ^{7}Be and the final abundance of ^{7}Li increases with baryon density.

2.1 Nuclear framework

The detailed prediction of the primordial abundances of various nuclei results from numerical computations that take into account a large network of nuclear reactions. There are several BBN codes publicly available, e.g. the PArthENoPE code (Public Algorithm Evaluating the Nucleosynthesis of Primordial Elements) [30] and the AlterBBN code [31]. Both of these codes are based on the first BBN codes by [32] and [29].

In the following we refer to the PArthENoPE code. It includes the evolution of 26 nuclides (see figure 2.2) and regards 100 reactions in total. An analysis of the reaction rates can be found in [33]. However, to obtain reliable results ($\leq 0.02\%$ difference) for

No.	Reaction
1	n decay
2	H+n $\rightarrow$ ^{2}H + γ
3	^{2}H + p $\rightarrow$ ^{3}He + γ
4	^{2}H + ^{2}H $\rightarrow$ ^{3}H + p
5	^{2}H + ^{2}H $\rightarrow$ ^{3}He + n
6	^{3}H + ^{2}H $\rightarrow$ ^{4}He + n
7	^{3}He + n $\rightarrow$ ^{3}H + p
8	^{3}He + ^{2}H $\rightarrow$ ^{4}He + p
9	^{3}H + ^{4}He $\rightarrow$ ^{7}Li + γ
10	^{3}He + ^{4}He $\rightarrow$ ^{7}Be + γ
11	^{7}Li + p $\rightarrow$ ^{4}He + ^{4}He
12	^{7}Be + n $\rightarrow$ ^{7}Li + p

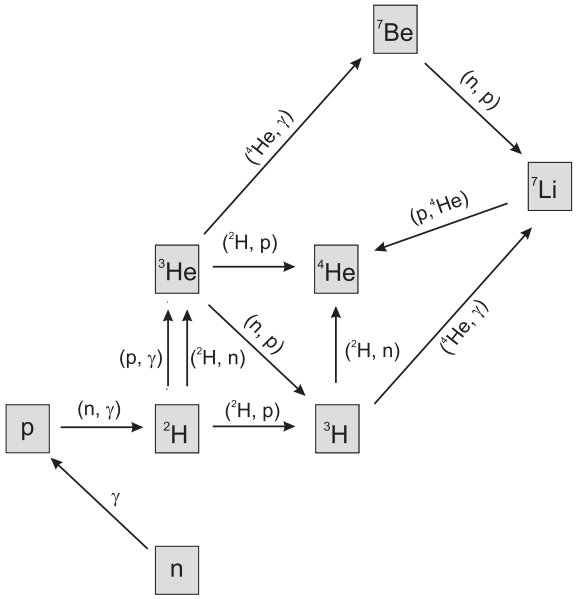

Figure 2.3: The twelve most important nuclear reactions controlling the primordial abundances of ^{2}H,^{3}He,^{4}He and ^{7}Li nuclides.

the abundances of ^{2}H, ^{3}He, ^{4}He and ^{7}Li a much smaller network of 9 nuclides and only 40 reactions is already sufficient. See table 2.3 for the 12 most important reactions.

The time evolution of the abundance of nucleus i during BBN is described by a set of reaction equations,

$$\dot{X}_i = \sum_{j,k,l} N_i \left(\Gamma_{kl\rightarrow ij} \frac{X_l^{N_l} X_k^{N_k}}{N_l! N_k!} - \Gamma_{ij\rightarrow kl} \frac{X_i^{N_i} X_j^{N_j}}{N_i! N_j!} \right) \equiv \hat{\Gamma}_i, \tag{2.6}$$

where $X_i = \frac{n_i}{n_b}$. N_i denotes the number of nuclei of type i in a given reaction and $\Gamma_{ij\rightarrow kl}$ denote the reaction rates. The ^{4}He abundance is described by $Y_{\mathrm{p}}^{\mathrm{BBN}} = 4X_{^4\mathrm{He}}$, which is slightly different from the definition of the helium mass fraction in (2.2). For the decay of species i, $\Gamma_{ij\rightarrow kl}$ must be replaced by the inverse mean life time of the nucleus $\Gamma_{i\rightarrow kl}$. For binary collisions, the reaction rate is given by the thermal average of the cross section for the reaction $i + j \rightarrow k + l$ times the relative velocity, i. e. $\Gamma_{ij\rightarrow kl} = \langle \sigma_{ij\rightarrow kl} v \rangle$. This quantity is in general temperature dependent and needs to be deduced from experimental data. Since some of the nuclear reaction rates have experimental errors up to $\sim 30\%$, they introduce a source of uncertainty in the predicted primordial abundances. Another source of uncertainty comes from the measurement of the neutron life time, which is constrained to $\tau_{\mathrm{n}} = [880.3 \pm 1.1]$ s by [27], but to $\tau_{\mathrm{n}} = [887.8 \pm 1.2^{(\mathrm{stat.})} \pm 1.9^{(\mathrm{syst.})}]$ s by [34]. The final error on Y_p is at the order of 10^{-4} (not taking into account the discrepancy between the two measurements of τ_{n} which

introduces another systematic error of $\mathcal{O}(10^{-3})$).

It is important to note that thermal equilibrium was explicitly assumed in equation (2.6). This seems to be a reasonable assumption for charged particles, because even though the newly formed nuclei have high kinetic energies, they will thermalize very fast by Coulomb scattering on the surrounding electrons. However, since neutrons do not Coulomb scatter, their thermalization time is much longer and it is doubtful whether thermal equilibrium can indeed be assumed. In general, these highly energetic neutrons could induce reactions that are otherwise thermally suppressed, see [35–37].

2.2 State of the art: prediction vs. observation

Observations of the cosmic microwave background (CMB) allow us to fix the baryon density to $\Omega_\mathrm{b}h^2 = 0.02225 \pm 0.00016$ [5]. In standard cosmology, no time variation of the number of baryons in a comoving volume is expected between the epoch of BBN at ~ 0.1 MeV and the formation of the CMB at ~ 0.3 eV. This allows us to fix the only free parameter in standard BBN and make predictions on the primordial abundances of light elements.

In a recent work [38] some updates on several reaction rates have been taken into account. The resulting predictions of Y_p, D/H, ^{3}He/H and ^{7}Li/H as well as their 1σ-uncertainties based on a Monte Carlo calculation can be found in table 2.1.

Until the formation of the first stars the primordial abundances of light nuclei are expected to stay unchanged. Afterwards, the nuclide abundances are modified by stellar processes. The exact evolution of light elements in stars is complicated and strongly depends on the assumed stellar model. Therefore, in order to measure primordial abundances of light elements we are in general restricted to the observation of very old, metal poor regions at high redshifts. In table 2.1 we present the measured abundances of ^{4}He, D, ^{3}He and ^{7}Li from [39–41].

The weakly bound deuterium has a relatively simple post-BBN evolution: It only gets destroyed in stellar processes. Any measurement of D can therefore be understood as a lower bound on its primordial abundance. Its monotonic and strong dependency on η_{10} makes deuterium a good choice to measure the baryon density $\Omega_\mathrm{b}h^2$. However, the almost identical absorption spectra of HI and DI (only differing by the different reduced masses) are a major complication for the measurement of D/H. To entirely exclude an accidental measurement of HI instead of DI requires knowledge about the velocity of the observed system. This limits the number of possible targets for the measurements of the primordial D abundance. As we can see in table 2.1, the consistency of the observed deuterium abundance and the predicted one is weak, with an agreement at the $\sim 2\sigma$

nuclide	Prediction	Observation
$Y_{\rm p}$	0.2484±0.0002 [38]	0.2449±0.0040 [39]
D/H ($\times 10^{-5}$)	2.45±0.05 [38]	2.53±0.04 [40]
^{3}He/H ($\times 10^{-5}$)	1.07±0.03 [38]	1.1±0.2 [41]
^{7}Li/H ($\times 10^{-10}$)	5.61±0.26 [38]	$1.58^{+0.35}_{-0.28}$ [43]

Table 2.1: Predicted ($\Omega_{\rm b}h^2 = 0.02225 \pm 0.00016$ [5], $\tau_{\rm n} = 880.3 \pm 1.1$ s [27]) and observed values for the abundances of various nuclides and their uncertainties (1σ).

level. Note that the given measurement of D/H [40] in table 2.1 is the up to date most precise measurement [1]. Earlier measurements of D/H had uncertainties higher by a factor of 5-10, see e.g. references in [42]. Either a reduction of the uncertainties of the nuclear reaction rates or a reduction in the observation uncertainty will hopefully reveal in the future if the measured deuterium is consistent with BBN predictions or not.

The evolution of ^{3}He after BBN is much more complicated than the one of deuterium and depends strongly on stellar and galactic evolution models. Measurements of ^{3}He are based on its emission from ionized regions inside our galaxy. We see in table 2.1 that the observation of the ^{3}He abundance is –within its large observational uncertainty– consistent with its predicted value.

The post-BBN evolution of ^{4}He is again relatively simple. Through cycles of generations of stars the ^{4}He abundance has increased from its primordial value. Its primordial abundance is inferred from observations of the helium emission lines from ionized extragalactic and low-metallicity regions. From table 2.1 we can see that the predicted ^{4}He abundance is in very good agreement with the observations (within $\sim 1\sigma$).

The overall trend of the post-BBN evolution of lithium is an increase of its abundance. Probes of the primordial lithium abundance stem from the observation of absorption spectra of very old and very metal-poor stars in our galaxy. A striking feature in table 2.1 is the fact that the predicted ^{7}Li abundance exceeds the observed one by a factor $3-4$. This significant ($\sim 9\sigma$) discrepancy persists already for a long time and is referred to as the *cosmological lithium problem* (see e.g. [44] for a review). Solutions to the lithium problem have been proposed from different directions, e.g. experimental uncertainties, revised nuclear physics and new physics including non-standard particles.

For some time, a second lithium problem has been discussed [45, 46]. Observations of the ^{6}Li atomic line in halo stars seemed to indicate that the observed ^{6}Li to ^{7}Li ratio would be orders of magnitudes higher than the predicted one. However, those results have been questioned afterwards and there is no detection of the primordial ^{6}Li abundance left, leaving therefore no evidence for a second lithium problem [47, 48].

[1] The authors already provided a similarly precise measurement of D/H in [42].

No	Reaction
1	^{7} Li + ^{3}H $\rightarrow$ ^{4}He + ^{6}He
2	^{3}H + ^{3}H $\rightarrow$ ^{6}He + γ
3	^{7}Li + ^{7}Li $\rightarrow$ ^{8}Be + ^{6}He
4	^{9}Be + ^{9}Be $\rightarrow$ ^{6}He + ^{12}C
5	^{4}He + 2n $\rightarrow$ ^{6}He + γ

Table 2.2: Production channels of ^{6}He.

2.3 Inclusion of Helium-6 into BBN

In this section we study how the inclusion of an additional nuclide, namely ^{6}He, into the BBN framework changes the prediction of the primordial abundances of light elements. This section shows the first original results that were derived within this thesis.

Even though there have been major improvements in the analysis of the nuclear reaction rates [33], the main results of BBN are based on the pioneering work by [32] in the 1960's. It is an interesting task to try to recover which nuclides and which reaction channels have to be taken into account in the BBN framework. By investigating the nuclide chart in figure 2.2 we try to find the scheme from which the 26 nuclides considered in the PArthENoPE code have been selected. We notice that only the more stable nuclides have been considered. This selection has been made for several reasons: First of all, only little experimental data about the very short living nuclides are available. Second, those unstable nuclides will eventually decay before they can interact with any other nuclide and burn to heavier nuclides. The selection criteria for the nuclear reactions involve a more careful study of the experimental data of the nuclear reaction rates. In general, it seems to be reasonable to concentrate on those two-body reactions that are of the form "nuclide+ (p/n/d/t/ ^{3}He/ ^{4}He)", because heavier nuclide abundances are strongly suppressed and so are their reactions.

While studying the nuclide chart in figure 2.2 the question arises why ^{6}He has not been included in the BBN framework. ^{6}He has a half life time of 807 ms and is therefore more stable than some other nuclides that are taken into account in the code. Its decay product is ^{6}Li, via ^{6}He $\rightarrow$ ^{6}Li + e^{-} ($Q_{\mathrm{m}} = 3.508$ MeV). In table 2.2 we present five possible production channels of ^{6}He. Among these processes reactions 3 and 4 seem to be less efficient, because they include only heavier nuclides whose abundances are strongly suppressed. Also reaction 5 is unlikely to be relevant, because it is a three-body reaction. We therefore study in the following the first two reactions of table 2.2, together with the decay process of ^{6}He.

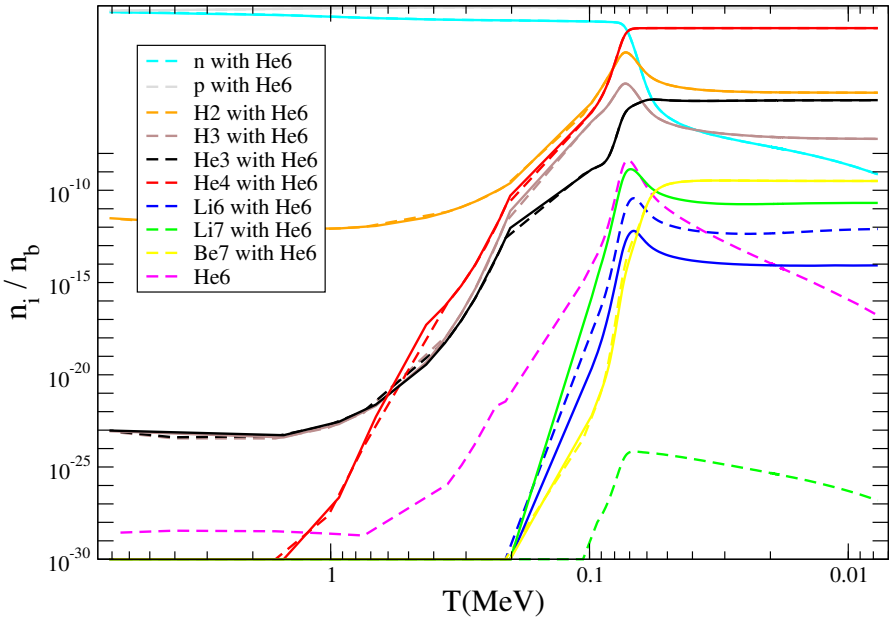

Figure 2.4: Nuclear abundances as a function of temperature T in MeV. Dashed lines include the production of ^{6}He by ^{7}Li + ^{3}H $\rightarrow$ ^{4}He + ^{6}He assuming a maximal reaction rate, solid lines are standard BBN. The neutron (light blue) dashed line is hidden behind the solid line.

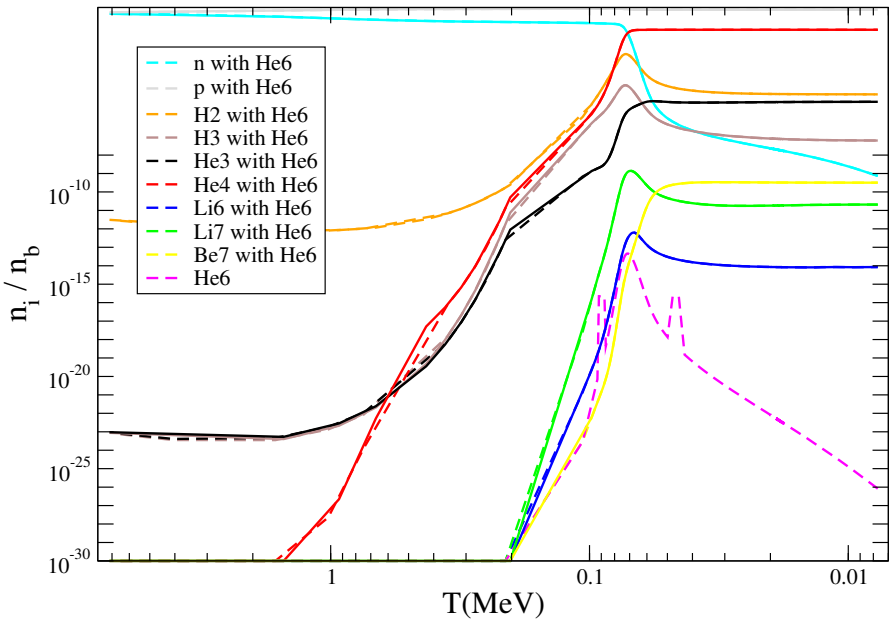

Figure 2.5: Same as figure 2.4, but with a more realistic reaction rate for ^{7}Li + ^{3}H $\rightarrow$ ^{4}He + ^{6}He, taken from [35].

^{7}Li + ^{3}H $\rightarrow$ ^{4}He + ^{6}He (Q_m=9.838 MeV) This reaction has the appealing feature that it destroys ^{7}Li and therefore potentially presents a way to weaken the lithium problem. First of all, we want to exploit the potential of this reaction by maximizing its impact and choosing the highest numerically possible reaction rate. The effect on the thermal evolution of the abundances of ^{7}Li (green) and ^{6}Li (blue) are shown in figure 2.4, with (solid) and without (dashed) inclusion of ^{6}He. As expected, the production of ^{7}Li is strongly suppressed when such a high reaction rate is assumed. The abundance of ^{6}He in contrast peaks at 0.1 MeV, decreasing afterwards by decay into ^{6}Li. The ^{6}Li abundance is therefore strongly enhanced and its abundance in the end of BBN is increased by roughly two orders of magnitude. If the second lithium problem would still persist, this would have been an interesting hint to follow. Naively one may expect that the primordial lithium abundance is entirely suppressed due to the strong suppression of its direct production. However, its final abundance is only reduced by less than 10% (not obvious from figure 2.4). This is due to the fact that most of the ^{7}Li is produced after BBN by electron capture of ^{7}Be, as explained in the beginning of this chapter. Therefore, in order to solve the lithium problem we have to find a mechanism that instead destroys ^{7}Be, which is mainly produced by ^{3}He + $\alpha \rightarrow \gamma$ + ^{7} Be.

It turned out that the authors of [35] have already considered the production of ^{6}He by the same reaction, ^{7}Li + ^{3}H $\rightarrow$ ^{4}He + ^{6}He. However, they used a more realistic reaction rate based on experimental data. As can be seen in figure 2.5, when using the same reaction rate as [35], ^{6}He is indeed produced, but its production is not efficient enough to have any impact on the ^{7}Li or ^{6}Li abundances. This result is compatible with the results of [35], up to the two spiky peaks in the ^{6}He curve in figure 2.5 that are most likely only numerical artefacts.

^{3}H + ^{3}H $\rightarrow \gamma$ + ^{6}He ($Q_\mathrm{m} = 12.308$ MeV) We could not find any experimental data on this reaction channel. However, in order to get an intuition for its possible impact on BBN we simply guess its nuclear reaction rate. At first, we decided to assume that its reaction rate is roughly the same as for the reaction ^{2}H + ^{2}H $\rightarrow$ ^{4}He + γ [32]. The results can be seen in figure 2.6. Similarly as in figure 2.5, ^{6}He is indeed produced, but its abundance stays so small that it does not have any impact on the abundance of ^{6}Li. In a next attempt, we assume the ^{3}H + ^{3}H $\rightarrow \gamma$ + ^{6}He reaction rate to be 10% of the total ^{3}H + ^{3}H reaction rate. As a matter of consistency, we reduce the ^{3}H + ^{3}H $\rightarrow$ 2n + ^{4}He reaction rate by about 10% at the same time. As we can see in figure 2.7, in this case a relatively large amount of ^{6}He is produced. The amount of ^{6}He even exceeds that of ^{7}Li at its maximum. Since all of the ^{6}He decays into ^{6}Li, the final abundance of ^{6}Li gets increased by a factor of ~ 4.5.

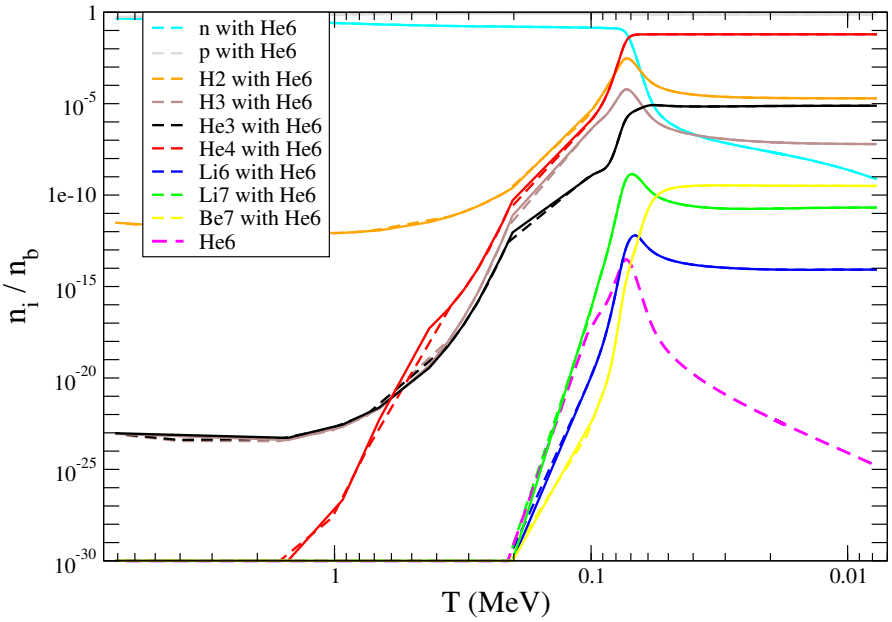

Figure 2.6: Nuclear abundances as a function of temperature T in MeV. Dashed lines include the reaction $^3H + {}^3H \rightarrow \gamma + {}^6He$ assuming the same reaction rate as for $^2H + {}^2H \rightarrow {}^4He + \gamma$, solid lines are standard BBN.

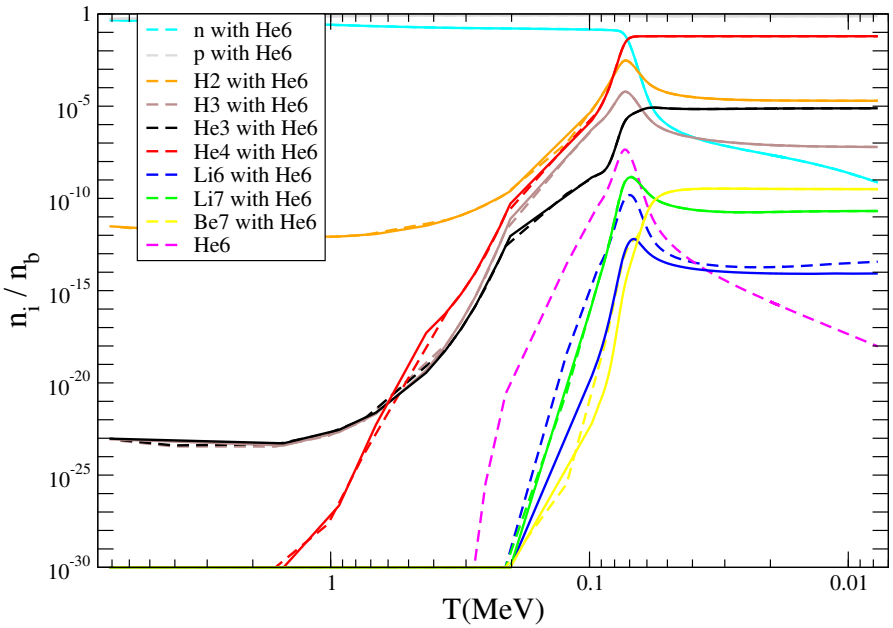

Figure 2.7: Same as figure 2.6, but with the reaction rate assumed to be 10% of the rate of the $^3H + {}^3H \rightarrow 2n + {}^4He$.

We end this section by concluding that ^{6}He is likely to be produced during BBN and has decayed into ^{6}Li afterwards. If the reaction ^{7}Li + ^{3}H $\rightarrow$ ^{4}He + ^{6}He is its only or most efficient production channel, its abundance has always been too low to have had any impact on the abundance of other light elements – unless the reaction rate has been strongly underestimated in [35]. If the reaction ^{3}H + ^{3}H $\rightarrow \gamma$ + ^{6}He is efficient as well, the decay of ^{6}He could have possibly enhanced the ^{6}Li abundance. In this case, there is also the chance that ^{6}He has been involved in further reactions (before its decay) that were not taken into account within this thesis. In principle, the inclusion of ^{6}He could therefore also have an impact on the abundances of other elements. Interesting reaction channels would for example be ^{6}He + ^{3}He $\rightarrow$ ^{3}H + ^{6}Li (possibly increasing the ^{6}Li abundance) and ^{6}He+ ^{4}He $\rightarrow$ ^{10}Be + γ (enhancing the primordial ^{10}B abundance by decay of ^{10}Be).

3 The cosmic microwave background

As we have seen in the previous chapter, the hot big bang theory is supported by the measurements of primordial elements which were formed long before the existence of the first stars, when the Universe was in an early hot and dense stage. Another consequence of the hot big bang theory is the fact that different particle species at early times must have been interacting with each other, forming the so called cosmic plasma. Atoms were ionized and photons were Thomson-scattering on free electrons, which made the Universe opaque to photons. Due to the expansion and cooling of the Universe different particle species have decoupled from the cosmic plasma at different times. Decoupling of neutrinos for example happened slightly before the onset of BBN, whereas photons remained coupled to electrons until the Universe was roughly 300,000 years old. At this time, electrons and nuclei combined to form neutral atoms and the Universe became transparent to photons. In chapter 3.1, we describe this recombination process in more detail.

Today, those free-streaming photons can be observed as the cosmic microwave background (CMB). Since photons travelled through the Universe relatively unhindered after decoupling (up to some secondary effects), the CMB is indeed a snapshot of the early Universe – the earliest snapshot that we can obtain [1]. Being formed when photons were in equilibrium, the CMB today shows an almost perfect blackbody spectrum with a temperature of $T_{\mathrm{CMB}} = 2.7255 \pm 0.0006$ K [49]. There are however tiny, direction dependent temperature fluctuations ($\Delta T/T \sim 10^{-5}$), see figure 3.1. Those temperature fluctuations are probably the most powerful cosmological measurement up to date in order to study the early Universe. The evolution of these temperature fluctuations is described within the framework of cosmic perturbation theory, which we introduce in section 3.2.

Let us briefly come back to the theory of inflation that we shortly introduced in section 1.3. As mentioned before, the uniformness of the CMB is another motivation for the inflationary paradigm. If there was nothing besides a radiation dominated era, followed by a matter dominated era and a recent entry into a dark energy dominated era, the CMB would consist of many patches that would have never been in causal contact

[1] A neutrino-snapshot from the neutrino decoupling epoch would be an even much earlier snapshot, but is unfortunately still out of reach with today's neutrino detectors.

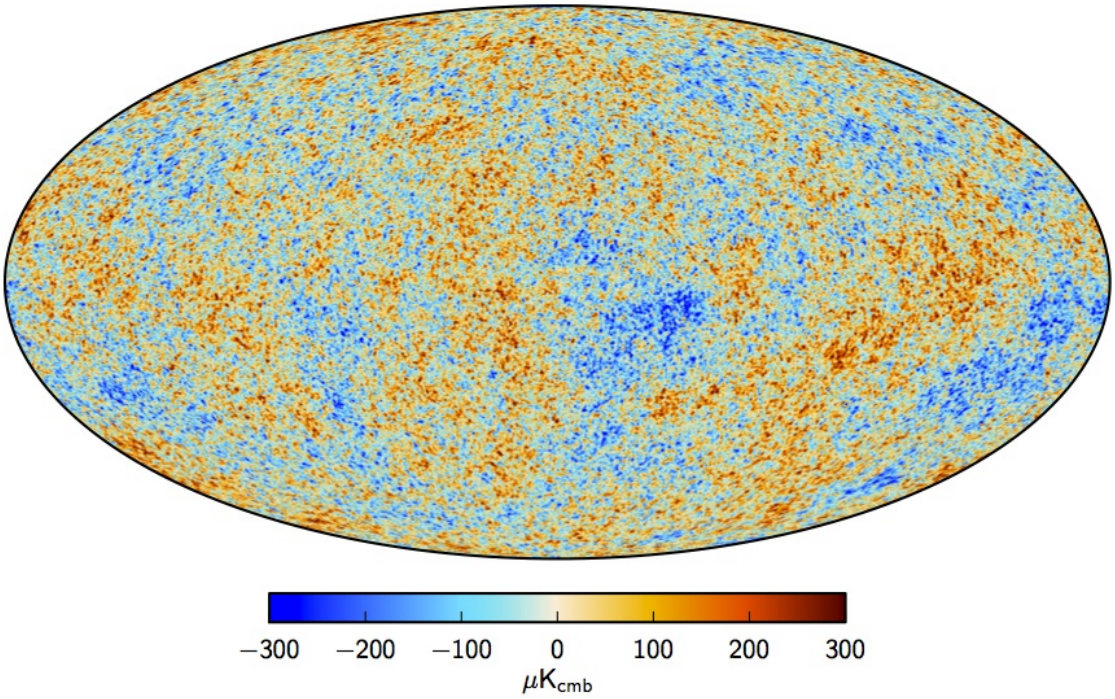

Figure 3.1: Map of the CMB temperature fluctuations, (credit: ESA and the Planck Collaboration).

before. But without ever being able to be in thermal contact, there is no reason why those patches should have the same temperature (*horizon problem*). The fact that the CMB looks almost the same in all direction can however be explained by the theory of inflation. The inflationary growth of space causes initially causally connected regions to become disconnected. The quantum fluctuations of the inflaton field(s) are furthermore the seeds for temperature fluctuations in the CMB and the structures we observe today [50–55].

3.1 Recombination

As mentioned above, the CMB was formed during recombination [2], when electrons and nuclei formed neutral atoms. Naively one may expect that recombination happened as soon as the temperature of the Universe fell below the binding energy of hydrogen (13.6 eV). However, similar to the delay of BBN, recombination was delayed due to the small baryon-to-photon ratio (2.4): High-energetic photons of the photon distribution tail destroyed any neutral atoms until the Universe was cooled down to $T \sim 0.3$ eV, as

[2] The term recombination is somewhat misleading, as it seems to indicate that the Universe has already been neutral at some point before, which is not the case.

we show on this section.

In the following, we want to quantitatively describe the recombination process. As we have seen in the previous chapter 2, most of the nucleons exist in form of hydrogen (protons) and helium, any other atoms are therefore neglected in the following.

As a first estimate, let us assume that equilibrium is maintained during recombination, such that all particles involved in the recombination process are described by their equilibrium distributions. Note that at the time scale of interest electrons and hydrogen atoms (neutral and ionized) are non-relativistic. In this case, we can write (Saha equation) [6–8]

$$\frac{n_{\mathrm{HII}}\, n_{\mathrm{e}}}{n_{\mathrm{HI}}} \approx \left(\frac{m_{\mathrm{e}} T}{2\pi}\right)^{3/2} \exp\left(-\frac{m_{\mathrm{e}} + m_{\mathrm{p}} - m_{\mathrm{H}}}{T}\right), \tag{3.1}$$

where n_{e} is the number density of *free* electrons. The sum in the exponent is simply given by the binding energy of hydrogen, $B_{\mathrm{H}} = m_{\mathrm{e}} + m_{\mathrm{p}} - m_{\mathrm{H}} = 13.6$ eV. By defining the free electron fraction as

$$x_{\mathrm{e}} \equiv \frac{n_{\mathrm{e}}}{n_{\mathrm{H}}} = \frac{n_{\mathrm{e}}}{n_{\mathrm{HI}} + n_{\mathrm{HII}}} \tag{3.2}$$

we can rewrite the Saha equation (3.1) as [7]

$$\begin{aligned} \frac{x_{\mathrm{e}}^2}{1 - x_{\mathrm{e}}} =& \frac{1}{n_{\mathrm{e}} + n_{\mathrm{HI}}} \left(\frac{m_{\mathrm{e}} T}{2\pi}\right)^{3/2} \exp\left(-\frac{B_{\mathrm{H}}}{T}\right) \\ =& \frac{10^{10}}{\eta_{10}(1 - Y_{\mathrm{p}})} \left(\frac{m_{\mathrm{e}}}{T}\right)^{3/2} \frac{\sqrt{\pi}}{2^{5/2}\zeta(3)} \exp\left(-\frac{B_{\mathrm{H}}}{T}\right). \end{aligned} \tag{3.3}$$

Here, we have explicitly neglected helium by assuming $n_{\mathrm{HII}} = n_{\mathrm{e}}$ (charge neutrality of the Universe) and furthermore used $n_{\mathrm{e}} + n_{\mathrm{HI}} \approx n_{\mathrm{b}}(1 - Y_{\mathrm{p}})$ and the definition of the baryon-to-photon ratio η_{10} (2.4). Equation (3.3) allows us to show that x_{e} drops to zero for $T \sim 0.3$ eV (using $Y_{\mathrm{p}} \approx 0.25$ and $\eta_{10} \approx 6$). Even though equation (3.3) is useful to get an estimate of the recombination temperature, it fails to describe the exact evolution of x_{e} as well as its correct asymptotic value. The reason for this is that the Saha equation (3.1) assumes perfect equilibrium during recombination. But when the number density of free electrons decreases, high-energetic photons emitted during the recombination process cannot thermalize any longer by scattering and the equilibrium condition breaks down. It is interesting to note that an analogous Saha equation (3.1) for helium gives in contrast a much more realistic picture of helium recombination (e.g. [56]). Due to its higher ionization energies (26.6 eV for HeI and 54.4 eV for HeII), helium recombination happens earlier than hydrogen recombination. Since there are more hydrogen atoms than helium atoms in the Universe, the assumption of equilibrium is indeed better justified during helium recombination, as there are still enough

free electrons to thermalize highly energetic photons even towards the end of helium recombination.

However, the correct formalism describing hydrogen recombination was first derived in 1968 by Peebles [57] and independently by Zel'dovich, Kurt and Sunyaev [58]. We do not go into the details of the derivation in the following, but rather sketch the most important physics that are incorporated in Peebles' recombination model. First of all, it is important to notice that direct recombination from the continuum to the ground state is never efficient, because it would lead to emission of a photon that would immediately reionize an atom in the surrounding. Therefore, recombination can only happen through an excited state. Neglecting higher excitation levels than n=2 for the moment, there are two excited states that can play a role during recombination. The $2s$ excited hydrogen state decays into the ground state via $2s \rightarrow 1s + 2\gamma$. Note that $2s \rightarrow 1s + \gamma$ is forbidden due to conservation of the angular momentum quantum number. Furthermore, the $2p$ state decays into the ground state via $2p \rightarrow 1s + \gamma$, but by emitting a Lyman-α photon this process eventually also excites a surrounding atom leading to no net recombination effect. This is also the reason why the $2p$ decay turns out to be less efficient for the bulk of recombination than the $2s$ decay, even though its decay rate is larger by orders of magnitude. Only when the free electron fraction is sufficiently low and the Lyman-α photons get redshifted, the $2s$ decay becomes important in order to finish the recombination process.

Finally, the equation describing the evolution of the number of free electrons is given by [57]

$$\frac{\mathrm{d}x_e}{\mathrm{d}t} = \left[\beta_c(1-x_e)e^{-E_{Ly\alpha}/T} - \alpha_c x_e^2 n_H\right] C\,, \tag{3.4}$$

where α_c is the coefficient for recombination into an excited state and β_c the photoionization rate of excited states. $E_{Ly\alpha}$ denotes the Lyman-α energy (10.2 eV) and the coefficient C is defined as

$$C = \frac{[1 + K\Lambda_{2s,1s} n_{1,s}]}{[1 + K(\Lambda_{2s,1s} + \beta_c) n_{1s}]}\,, \tag{3.5}$$

where $\Lambda_{2s,1s}$ is the decay rate of the $2s$ state and K takes into account the redshift of the Lyman-α photons,

$$K = \frac{\lambda_{Ly\alpha}^3}{8\pi H(t)}. \tag{3.6}$$

The relatively simple recombination model by Peebles is remarkably successful in describing the recombination process in the early Universe. It however also has some shortcomings as it makes use of some simplifying assumptions, e.g. it neglects helium entirely, assumes that excited states are in equilibrium with radiation and collisional

ionizations are negligible. Today's recombination codes take into account corrections to most of these shortcomings and include the evolution equations of hundreds of excited hydrogen states (Recfast [56], CosmoRec [59, 60], HyRec [61]).

Let us end this section with a final remark. To finally find the redshift at which photons stopped scattering off electrons, we need to insert the free electron fraction into the Thomson scattering rate and compare the latter to the Hubble expansion rate. This gives a photon decoupling redshift of roughly $z \approx 1100$. If there would be no recombination (which is certainly a hypothetical scenario), photons would remain scattering off electrons until much later times, $z_{\rm dec} \approx 40$ [8]. This is interesting to notice, because our Universe gets ionized again at some later time during the epoch of reionization. Our work in chapter 4 is related to this epoch and goes into some more detail about it. If the Universe already got reionized before $z_{\rm dec} \approx 40$, photons and free electrons would thermalize again, which would entirely suppress the CMB anisotropies that we study in the next section. However, current astrophysical observations seem to indicate that reionization happened around $z \sim 10$, which makes the impact of reionization on the CMB less dramatic.

3.2 Cosmic perturbation theory

In this section, we summarize the theoretical framework describing the evolution of the CMB temperature fluctuations. A complete and detailed description of cosmic perturbation theory is beyond the scope of this work, but can be found e.g. in [62] and standard text books as [8–10]. We follow the widely used notation of [62] in the following.

The cosmological principle states that our Universe is homogeneous and isotropic. But there were small perturbations to homogeneity and isotropy – perturbations that have risen from quantum fluctuations of the inflaton field. We can describe those perturbations by a perturbed metric (at linear order),

$$g_{\mu\nu} = \bar{g}_{\mu\nu} + a^2 h'_{\mu\nu}\,, \tag{3.7}$$

where in general

$$h'_{\mu\nu}\mathrm{d}x^\mu \mathrm{d}x^\nu = -2A\,\mathrm{d}\tau^2 - 2B_i\,\mathrm{d}\tau \mathrm{d}x^i + 2H_{ij}\,\mathrm{d}x^i \mathrm{d}x^j. \tag{3.8}$$

There are two important aspects concerning the perturbed metric $h'_{\mu\nu}$ which we only want to mention briefly here. First of all, the 10 components of the metric (3.8) can be decomposed into scalar (four components), vector (four components) and tensor modes

(two components). At linear order in $h'_{\mu\nu}$, there is no coupling between those different modes. Since we are at this point only interested in scalar fluctuations, e.g. temperature or density fluctuations, we only consider the evolution of scalar perturbations in the following.

Furthermore, there is no unique choice of a coordinate system in a perturbed space time. Therefore, with an infinitesimal coordinate transformation we can eliminate two of the scalar components (and two of the vector components), leaving only two physical degrees of freedom for scalar perturbations. In the following we focus on the *synchronous* gauge, in which A as well as the scalar part of B_i in (3.8) are set to zero, such that the line element can be written (in terms of conformal time) as

$$\mathrm{d}s^2 = a^2(\tau)\left(-\mathrm{d}\tau^2 + (\delta_{ij} + h_{ij})\,\mathrm{d}x^i \mathrm{d}x^j\right)\,, \tag{3.9}$$

where the perturbed metric is given in terms of its trace h and a scalar field μ,

$$h_{ij} = h\frac{\delta_{ij}}{3} + \left(\partial_i\partial_j - \frac{1}{3}\delta_{ij}\nabla^2\right)\mu\,. \tag{3.10}$$

The synchronous gauge (3.10) does however still leave some gauge freedom which we will fix later in this section.

Likewise, the energy-momentum tensor is not exactly that of a perfect fluid anymore, but has perturbations such that it can be written as

$$\begin{aligned} T^0{}_0 &= -(\bar{\rho} + \delta\rho), \\ T^0{}_i &= (\bar{\rho} + \bar{\mathcal{P}})v_i = -T^i{}_0, \\ T^i{}_j &= (\bar{\mathcal{P}} + \delta\mathcal{P})\delta^i{}_j + \Sigma^i{}_j, \qquad \text{with } \Sigma^i{}_i = 0. \end{aligned} \tag{3.11}$$

We can now derive the perturbed Einstein tensor in the synchronous gauge (3.9). It turns out to be useful to work in Fourier space, where the perturbed metric (3.10) is described by the two fields $h(\boldsymbol{k},\tau)$ and $\eta(\boldsymbol{k},\tau)$,

$$h_{ij}(\boldsymbol{x},\tau) = \int \mathrm{d}^3k\, e^{i\boldsymbol{k}\cdot\boldsymbol{x}}\left[\delta_{ij}\,h(\boldsymbol{k},\tau) + \left(\hat{\boldsymbol{k}}_i\hat{\boldsymbol{k}}_j - \frac{1}{3}\delta_{ij}\right)6\eta(\boldsymbol{k},\tau)\right], \qquad \boldsymbol{k} = k\hat{\boldsymbol{k}}\,. \tag{3.12}$$

Here, h denotes the trace of h_{ij} in real *and* in Fourier space ($\tilde{h} \equiv h(\boldsymbol{k},\tau)$) and η is related to the Fourier transform of μ (3.10) by $6\eta = -k^2\tilde{\mu}$.

The components of the perturbed Einstein equation are then given by

$$k^2\eta - \frac{1}{2}\frac{\dot{a}}{a}\dot{h} = 4\pi G a^2\delta\rho, \tag{3.13}$$

$$k^2\dot{\eta} = 4\pi G a^2(\bar{\rho} + \bar{\mathcal{P}})\theta, \tag{3.14}$$

$$\ddot{h} + 2\frac{\dot{a}}{a}\dot{h} - 2k^2\eta = -8\pi G a^2 \delta\mathcal{P}, \tag{3.15}$$

$$\ddot{h} + 6\ddot{\eta} + 2\frac{\dot{a}}{a}\left(\dot{h} + 6\dot{\eta}\right) - 2k^2\eta = -24\pi G a^2(\bar{\rho} + \bar{\mathcal{P}})\sigma, \tag{3.16}$$

where we defined

$$\theta = ik^j v_j \quad \text{and} \quad (\bar{\rho} + \bar{\mathcal{P}})\sigma = -(\hat{k}_i\hat{k}_j - \frac{1}{3}\delta_{ij})\Sigma^i{}_j. \tag{3.17}$$

The evolution of the background metric $g_{\mu\nu}$ follows simply from the Friedmann equation (1.7) and the continuity equation (1.8).

The advantage of working in Fourier space is that the perturbed Einstein equation simplifies from a set of partial differential equations to a set of ordinary differential equations in (3.13)-(3.16). At linear order in perturbation theory, these differential equations can be solved for each individual k mode, i.e. there is no coupling between different k modes.

At the times of interest, the Universe is filled with four relevant particle species: photons, baryons (including electrons and nuclei), dark matter and neutrinos. The Einstein equations (3.13)-(3.16) contain on the r.h.s. a sum over all of those different particle species. Each individual particle species is however described by its perturbed phase space density $f_i(\boldsymbol{k}, \boldsymbol{P}, \tau)$, where $\boldsymbol{P}$ is the four-momentum (as in section 1.2). It is however more convenient to write the phase space perturbation in terms of comoving momentum $\boldsymbol{q} = a\boldsymbol{p}$ (with $\boldsymbol{p}$ being the physical momentum),

$$f_i(\boldsymbol{k}, \boldsymbol{P}, \tau) = \bar{f}_i(q)\left(1 + \Psi_i(\boldsymbol{k}, \boldsymbol{q}, \tau)\right), \tag{3.18}$$

where $q = |\boldsymbol{q}|$ and $\bar{f}(q)$ is the equilibrium distribution.

The evolution of the phase space density (3.18) is described by the Boltzmann equation (1.13). For the Liouville operator on the l.h.s. we need to calculate the perturbed Christoffel symbols ($\Gamma^\nu_{\rho\sigma} + \delta\Gamma^\nu_{\rho\sigma}$) of the metric (3.9), changing thereby from four-momentum $\boldsymbol{P}$ to comoving momentum $\boldsymbol{q}$. The perturbed Boltzmann equation at linear order is then finally given by

$$\frac{\partial\Psi_i}{\partial\tau} + ik\frac{q}{\epsilon}(\hat{\boldsymbol{k}}\cdot\hat{\boldsymbol{q}})\Psi_i + \frac{\mathrm{d}\ln\bar{f}_i}{\mathrm{d}\ln q}\left[\dot{\eta} - \frac{\dot{h} + 6\dot{\eta}}{2}(\hat{\boldsymbol{k}}\cdot\hat{\boldsymbol{q}})^2\right] = \frac{1}{\bar{f}_i}\mathcal{C}^1(f_i). \tag{3.19}$$

Here, $\hat{\boldsymbol{k}}$ and $\hat{\boldsymbol{q}}$ are the normal vectors of $\boldsymbol{k}$ and $\boldsymbol{q}$, and $\mathcal{C}^1$ is the perturbed collision integral at linear order.

As we can see from the Boltzmann equation (3.19), the phase space perturbation Ψ depends on conformal time τ, the absolute value of the wave vector k, the absolute

value of the comoving momentum q, as well as on the cosine of the angle between those two vectors, $\hat{\boldsymbol{k}} \cdot \hat{\boldsymbol{q}}$. In order to solve the Boltzmann equation numerically it is convenient to expand Ψ in a Legendre series,

$$\Psi_i(k, q, \hat{\boldsymbol{k}} \cdot \hat{\boldsymbol{q}}, \tau) = \sum_{\ell=0}^{\infty} (-i)^\ell (2\ell + 1) \Psi_{i,\ell}(k, q, \tau) P_\ell(\hat{\boldsymbol{k}} \cdot \hat{\boldsymbol{q}}), \tag{3.20}$$

where $\Psi_{i,\ell}(k, q, \tau)$ denotes the ℓth multipole,

$$\Psi_{i,\ell}(k, q, \tau) = \frac{1}{2(-i)^\ell} \int_{-1}^{1} \mathrm{d}(\hat{\boldsymbol{k}} \cdot \hat{\boldsymbol{q}})\, \Psi_i(k, q, \hat{\boldsymbol{k}} \cdot \hat{\boldsymbol{q}}, \tau) P_\ell(\hat{\boldsymbol{k}} \cdot \hat{\boldsymbol{q}}). \tag{3.21}$$

The components of the perturbed energy-momentum tensor are given by integrals of the multipoles over momentum,

$$\delta\rho_i = 4\pi a^{-4} \int \mathrm{d}q\, q^2 \epsilon \bar{f}_i(q) \Psi_{i,0}, \tag{3.22}$$

$$\delta P_i = \frac{4\pi}{3} a^{-4} \int \mathrm{d}q\, \frac{q^4}{\epsilon} \bar{f}_i(q) \Psi_{i,0}, \tag{3.23}$$

$$(\bar{\rho}_i + \bar{P}_i)\theta_i = 4\pi k a^{-4} \int \mathrm{d}q\, q^3 \bar{f}_i(q) \Psi_{i,1}, \tag{3.24}$$

$$(\bar{\rho}_i + \bar{P}_i)\sigma_i = \frac{8\pi}{3} a^{-4} \int \mathrm{d}q\, \frac{q^4}{\epsilon} \bar{f}_i(q) \Psi_{i,2}, \tag{3.25}$$

where ϵ denotes the comoving energy, $\epsilon = \sqrt{q^2 + a^2 m^2}$. Let us for the moment focus on neutrinos, which decouple long before recombination and are therefore non-interacting at the times of interest. In chapter 5 we study a scenario in which neutrinos have non-standard interactions that are possibly still efficient at recombination time. This necessitates the calculation of a collision integral $\mathcal{C}^1$ that takes into account those new type of interactions. For standard weakly interacting neutrinos the collision integral $\mathcal{C}^1$ on the r.h.s. of the Boltzmann equation (3.19) is however zero. The Legendre expansion (3.20) is now inserted into the collisionless Boltzmann equation (3.19). After integrating it over $\int \mathrm{d}(\hat{\boldsymbol{k}} \cdot \hat{\boldsymbol{q}}) P_\ell(\hat{\boldsymbol{k}} \cdot \hat{\boldsymbol{q}})[...]$ and using the orthogonality relation of the Legendre polynomials

$$\int \mathrm{d}(\hat{\boldsymbol{k}} \cdot \hat{\boldsymbol{q}})\; P_\ell(\hat{\boldsymbol{k}} \cdot \hat{\boldsymbol{q}}) \cdot P_n(\hat{\boldsymbol{k}} \cdot \hat{\boldsymbol{q}}) = \frac{2}{2\ell + 1} \delta_{\ell n} \tag{3.26}$$

we find a set of coupled differential equations for the multipoles (for each neutrino mass state), the so called Boltzmann hierarchy for neutrinos,

$$\dot{\Psi}_{\nu,0} = -\frac{qk}{\epsilon} \Psi_{\nu,1} + \frac{1}{6} \dot{h} \frac{\mathrm{d} \ln \bar{f}_\nu}{\mathrm{d} \ln q}, \tag{3.27}$$

$$\dot{\Psi}_{\nu,1} = \frac{qk}{3\epsilon}(\Psi_{\nu,0} - 2\Psi_{\nu,2}), \tag{3.28}$$

$$\dot{\Psi}_{\nu,2} = \frac{qk}{5\epsilon}(2\Psi_{\nu,1} - 3\Psi_{\nu,3}) - \left(\frac{1}{15}\dot{h} + \frac{2}{5}\dot{\eta}\right)\frac{\mathrm{d}\ln\bar{f}_\nu}{\mathrm{d}\ln q}, \tag{3.29}$$

$$\dot{\Psi}_{\nu,\ell} = \frac{qk}{(2\ell+1)\epsilon}\left(\ell\Psi_{\nu,\ell-1} - (\ell+1)\Psi_{\nu,\ell+1}\right),\ \ell \geq 3. \tag{3.30}$$

The Boltzmann hierarchy (3.27)-(3.30) is entirely equivalent to the Boltzmann equation (3.19), but instead of depending on the (continuous) angle $\hat{\boldsymbol{k}} \cdot \hat{\boldsymbol{q}}$ it is a set of infinitely many coupled differential equations. Since the Legendre polynomials have an oscillatory behaviour for large ℓ, multipoles (3.21) with large ℓ are suppressed compared to those with low ℓ. It therefore seems to be a reasonable approximation to cut the hierarchy at some ℓ_{max}.

For massless neutrinos ($q = \epsilon$) the momentum dependence in (3.27)-(3.30) can be integrated out by introducing

$$F_\nu(k, \hat{\boldsymbol{k}} \cdot \hat{\boldsymbol{q}}, \tau) \equiv \frac{\int \mathrm{d}q\, q^3 \bar{f}_\nu \Psi_\nu}{\int \mathrm{d}q\, q^3 \bar{f}_\nu} \equiv \sum_{\ell=0}^{\infty}(-i)^\ell(2\ell+1)F_{\nu,\ell}(k,\tau)P_\ell(\hat{\boldsymbol{k}} \cdot \hat{\boldsymbol{q}}). \tag{3.31}$$

This allows to rewrite the Boltzmann hierarchy for massless neutrinos as

$$\dot{\delta}_\nu = -\frac{4}{3}\theta_\nu - \frac{2}{3}\dot{h}, \tag{3.32}$$

$$\dot{\theta}_\nu = k^2\left(\frac{1}{4}\delta_\nu - \sigma_\nu\right), \tag{3.33}$$

$$\dot{F}_{\nu,2} = 2\dot{\sigma}_\nu = \frac{8}{15}\theta_\nu - \frac{3}{5}kF_{\nu,3} + \frac{4}{15}\dot{h} + \frac{8}{5}\dot{\eta}, \tag{3.34}$$

$$\dot{F}_{\nu,\ell} = \frac{k}{2\ell+1}\left(\ell F_{\nu,\ell-1} - (\ell+1)F_{\nu,\ell+1}\right),\ \ell \geq 3, \tag{3.35}$$

where $\delta_\nu = \delta\rho_\nu/\rho_\nu$.

Due to its momentum dependence the Boltzmann hierarchy for massive neutrinos (3.27)-(3.30) is computationally more expensive than the one for massless neutrinos (3.33)-(3.35). It has to be solved on a momentum grid and its contribution to the Einstein equation is obtained by momentum integration according to equations (3.22)-(3.25).

For the sake of completeness we also want to summarize the Boltzmann equations of photons, baryons and dark matter. In contrast to the neutrino Boltzmann hierarchy (3.27)-(3.35), the photon Boltzmann hierarchy contains a collision integral that takes into account Thomson scattering between photons and baryons,

$$\dot{\delta}_\gamma = -\frac{4}{3}\theta_\gamma - \frac{2}{3}\dot{h}, \tag{3.36}$$

$$\dot{\theta}_\gamma = k^2\left(\frac{1}{4}\delta_\gamma - \sigma_\gamma\right) + an_\mathrm{e}\sigma_\mathrm{T}(\theta_\mathrm{b} - \theta_\gamma), \tag{3.37}$$

$$\dot{F}_{\gamma,2} = 2\dot{\sigma}_\gamma = \frac{8}{15}\theta_\gamma - \frac{3}{5}kF_{\gamma,3} + \frac{4}{15}\dot{h} + \frac{8}{5}\dot{\eta} - \frac{9}{5}an_\mathrm{e}\sigma_\mathrm{T}\sigma_\gamma + \frac{1}{10}an_\mathrm{e}\sigma_\mathrm{T}(G_{\gamma,0} + G_{\gamma,2}), \tag{3.38}$$

$$\dot{F}_{\gamma,\ell} = \frac{k}{2\ell+1}\left(\ell F_{\gamma,\ell-1} - (\ell+1)F_{\gamma,\ell+1}\right) - an_\mathrm{e}\sigma_\mathrm{T}F_{\gamma,\ell},\ \ell \geq 3, \tag{3.39}$$

$$\begin{aligned}\dot{G}_{\gamma,\ell} =& \frac{k}{2\ell+1}\left(\ell G_{\gamma,\ell-1} - (\ell+1)G_{\gamma,\ell+1}\right) \\ &+ an_\mathrm{e}\sigma_\mathrm{T}\left(-G_{\gamma,\ell} + \frac{1}{2}(F_{\gamma,2} + G_{\gamma,0} + G_{\gamma,2})\left(\delta_{\ell 0} + \frac{\delta_{\ell 2}}{5}\right)\right).\end{aligned} \tag{3.40}$$

Here σ_T denotes the Thomson scattering cross section, a is the scale factor and n_e the number density of free electrons. Furthermore, $F_{\gamma,\ell}$ is defined analogously to (3.31) and $G_{\gamma,\ell}$ is the ℓth multipole of the difference between the two linear polarization components of photons. Due to the coupling of $F_{\gamma,\ell}$ and $G_{\gamma,\ell}$ at $\ell = 2$ the CMB polarization depends mainly on the temperature quadrupole moment $F_{\gamma,2}$.

Thomson scattering introduces a damping term $\propto -F_{\gamma,\ell}$ at $\ell \geq 1$ in the photon hierarchy. At early times – when scattering between electrons and photons is very efficient – this damping term suppresses multipoles larger than the dipole (tightly coupled limit). Of course, the validity of the tightly coupled limit depends also on the wave vector k and works better for large scales (small k) than for small scales (large k). After recombination however the damping term is negligible and photons start free-streaming, which populates the higher multipoles.

We furthermore see in (3.37) that the photon velocity divergence θ_γ is coupled directly to the baryon velocity divergence θ_b due to Thomson scattering. As we will see in the following, the baryon hierarchy shows in turn a similar coupling at $\ell = 1$.

In the Boltzmann hierarchy for non-relativistic particles, i.e. baryons and cold dark matter, all multipoles with $\ell \geq 2$ are suppressed ($\propto q/\epsilon \ll 1$). The baryon equations are then given by

$$\dot{\delta}_\mathrm{b} = -\theta_\mathrm{b} - \frac{1}{2}\dot{h}, \tag{3.41}$$

$$\dot{\theta}_\mathrm{b} = -\frac{\dot{a}}{a}\theta_\mathrm{b} + c_\mathrm{s}^2k^2\delta_\mathrm{b} + \frac{4\bar{\rho}_\gamma}{3\bar{\rho}_\mathrm{b}}an_\mathrm{e}\sigma_\mathrm{T}(\theta_\gamma - \theta_\mathrm{b}). \tag{3.42}$$

Like neutrinos, dark matter is non-interacting at the times of interest and therefore has no collision integral on the r.h.s. of the Boltzmann equation (3.19). As mentioned before, there is still some gauge freedom in the synchronous gauge (3.10), which we fix by setting $\theta_\mathrm{c} = 0$. Cold dark matter is then described by a single equation, i.e.

$$\dot{\delta}_\mathrm{c} = -\frac{1}{2}\dot{h}. \tag{3.43}$$

The Boltzmann hierarchies of photons (3.36)-(3.40), neutrinos (3.27)-(3.35), baryons (3.41)-(3.42) and cold dark matter (3.43) are all coupled to each other via the perturbed Einstein equations (3.13)-(3.16) and represent the theoretical framework that describes the formation of the CMB. In order to make any predictions we also have to impose initial conditions, which we do not show here explicitly but which can be found in [62]. Of course, cosmic perturbation theory cannot predict how the CMB sky exactly looks like today, i.e. which region in the sky is hotter or colder than the average. We can only make predictions about the statistical distribution of the temperature fluctuations which is described by the angular power spectrum that we introduce in the following.

Let us first explain the angular power spectrum from the observational point of view. The photon phase space perturbation $\Psi_\gamma(\boldsymbol{x}, \hat{\boldsymbol{q}}, \tau)$ (3.18) can be related to a perturbation of the CMB temperature $\Delta = \Delta T/T$,

$$f_\gamma(\boldsymbol{x}, \boldsymbol{q}, \tau) = \frac{1}{\exp\left(\frac{q}{T(1+\Delta)}\right) - 1} \approx \bar{f}_\gamma(q) - q\frac{\mathrm{d}\bar{f}_\gamma}{\mathrm{d}q}\Delta, \tag{3.44}$$

where we have expanded f_γ up to first order in $\Delta = 0$. Comparing this expression (3.44) to equation (3.18) we find the following relation for Δ,

$$\Delta = -\left(\frac{\mathrm{d}\ln\bar{f}_\gamma}{\mathrm{d}\ln q}\right)^{-1}\Psi_\gamma. \tag{3.45}$$

Inserting this relation into the perturbed Boltzmann equation (3.19) reveals that Δ is a function of τ, x and $\hat{\boldsymbol{q}}$, but is *independent* of the magnitude of the comoving momentum q, since the $\frac{\mathrm{d}\ln\bar{f}_\gamma}{\mathrm{d}\ln q}$ term factorizes out. This allows to derive a simple relation between the temperature fluctuation Δ and F_γ (3.31),

$$\Delta = \frac{1}{4}F_\gamma \qquad \Rightarrow \Delta_\ell = \frac{1}{4}F_{\gamma,\ell}. \tag{3.46}$$

In practice, what we observe are temperature fluctuations Δ^{obs} in the direction $\hat{\boldsymbol{n}}$ measured *now* (on cosmological time scales) and *here* (on cosmological distances). A temperature fluctuation observed in direction $\hat{\boldsymbol{n}}$ refers to photons travelling in direction $-\hat{\boldsymbol{n}}$. Choosing our observer location as the origin ($\boldsymbol{x} = \boldsymbol{0}$) and specifying $\tau = \tau_0$ we find $\Delta^{\mathrm{obs}}(\hat{\boldsymbol{n}}) = \Delta(\boldsymbol{0}, \tau_0, -\hat{\boldsymbol{n}})$, which we decompose into a series of spherical harmonics [7],

$$\Delta^{\mathrm{obs}}(\hat{\boldsymbol{n}}) = \sum_{\ell=0}^{\infty}\sum_{m=-\ell}^{\ell} a_{\ell m}Y_{\ell m}(\hat{\boldsymbol{n}}), \quad a_{\ell m} = (-1)^\ell\int \mathrm{d}\Omega\, Y^*_{\ell m}(\hat{\boldsymbol{n}})\Delta(\boldsymbol{0}, \tau_0, \hat{\boldsymbol{n}}). \tag{3.47}$$

Here, we have performed a change of variable $\hat{\boldsymbol{n}} \to -\hat{\boldsymbol{n}}$ and used $Y_{\ell m}(-\hat{\boldsymbol{n}}) = (-1)^\ell Y_{\ell m}(\hat{\boldsymbol{n}})$

in the second equation. In terms of the temperature fluctuation Δ in Fourier space the $a_{\ell m}$ are given by (without proof here) [7]

$$a_{\ell m} = (-i)^\ell \int \frac{\mathrm{d}^3 k}{2\pi^2}\, Y^*_{\ell m}(\hat{\boldsymbol{k}}) \Delta_\ell(\tau_0, \boldsymbol{k}). \tag{3.48}$$

Under the assumption of isotropy and Gaussianity (predicted from inflation), the angular power spectrum is finally defined by the covariance matrix of the coefficients $a_{\ell m}$,

$$\langle a_{\ell m} a^*_{\ell' m'} \rangle = C_\ell\, \delta_{\ell\ell'}\, \delta_{mm'}. \tag{3.49}$$

The angle brackets in equation (3.49) denote a theoretical ensemble average, i.e. an average over many realizations of the CMB sky. But as we can only observe *one* realization which is the Universe we live in, we cannot take such an ensemble average in practice. Instead, we calculate the C_ℓ's from the $2\ell + 1$ *measured* coefficients $a_{\ell m}$ in our Universe,

$$C_\ell^{\text{obs}} = \frac{1}{2\ell + 1} \sum_{m=-\ell}^{\ell} |a_{\ell m}|. \tag{3.50}$$

This also implies that the C_ℓ's have an intrinsic uncertainty due to the limited number of coefficients $a_{\ell m}$ for a given ℓ in our Universe. This intrinsic uncertainty is more pronounced at low ℓ and is called *cosmic variance*,

$$\frac{\Delta C_\ell}{C_\ell} = \sqrt{\frac{2}{2\ell + 1}}. \tag{3.51}$$

The angular power spectrum (3.50) can be extracted from CMB maps (figure 3.1) by use of software packages like HEALPix[3] [63].

On the theoretical side, we can predict the angular power spectrum by using Boltzmann codes like CLASS [64][4] or CAMB [65][5] which numerically solve the Boltzmann hierarchies of photons (3.36)-(3.40), neutrinos (3.27)-(3.35), baryons (3.41)-(3.42) and dark matter (3.43) together with the perturbed Einstein equations (3.13)-(3.16). The (ensemble averaged) angular power spectrum (3.49) is then calculated according to

$$C_\ell = \frac{1}{2\pi^2} \int \frac{\mathrm{d}k}{k}\, \Delta^2_\ell(\tau_0, k) P_i(k), \tag{3.52}$$

[3] http://healpix.sourceforge.net
[4] http://class-code.net/
[5] http://camb.info

$\Omega_{\mathrm{b}}h^2$	The density of baryons, defined according to (1.11).
$\Omega_{\mathrm{c}}h^2$	The density of cold dark matter, defined according to (1.11).
$100\theta_{\mathrm{MC}}$	The sound horizon at last scattering.
τ_{reio}	The optical depth due to reionization.
$\ln\left(10^{10}A_{\mathrm{s}}\right)$	The amplitude of the primordial power spectrum, see (3.54).
n_{s}	The tilt of the primordial power spectrum, see (3.54).

Table 3.1: The six free parameters of the ΛCDM model.

where $P_i(k)$ is the primordial power spectrum, defined as

$$\langle \Delta_\ell(\tau, \boldsymbol{k}) \Delta_\ell^*(\tau, \boldsymbol{k'}) \rangle = \frac{2\pi^3}{k^3} P_i(k) \delta^{(3)}(\boldsymbol{k} - \boldsymbol{k'}) [\Delta_\ell(\tau, k)]^2. \tag{3.53}$$

Inflation predicts a (nearly) scale-invariant power spectrum, which is characterized by the spectral index n_{s} (with $n_{\mathrm{s}} = 1$ implying exact scale invariance) and the primordial amplitude A_{s},

$$P_i(k) = A_{\mathrm{s}} \left(\frac{k}{k_0} \right)^{n_{\mathrm{s}}-1}, \tag{3.54}$$

where k_0 is an arbitrary pivot scale.

Modern Boltzmann codes like CLASS and CAMB are based on the line of sight approach [66]. The introduction of this approach drastically reduced the required number of equations in the photon Boltzmann hierarchy (ℓ_{max}) in order to calculate the angular power spectrum (3.52) and was therefore a major progress in terms of numerical computation time.

3.3 Observation of the cosmic microwave background

Our predictions for the CMB angular power spectrum (3.52) of course depend on several parameters. The flat ΛCDM model has six independent free parameters (base parameters) that are summarized and described in table 3.1. It explicitly assumes zero curvature and no other relativistic particles than photons and three flavours of neutrinos. All other cosmological parameters, e.g. the Hubble constant H_0 (1.5) or the cosmological constant density Ω_Λ (1.11), can be derived from the six base parameters 3.1. Some of the base parameters are of course degenerate, i.e. the signal in the angular power spectrum induced by the variation of one parameter can be mimicked by the variation of one or several other parameters.

The first detection of the CMB goes back to 1964, when A. Penzias and R. W. Wilson detected it by accident as they used a radiometer to perform radio astronomy and communication experiments (Nobel prize 1987). The CMB temperature *anisotropies* were

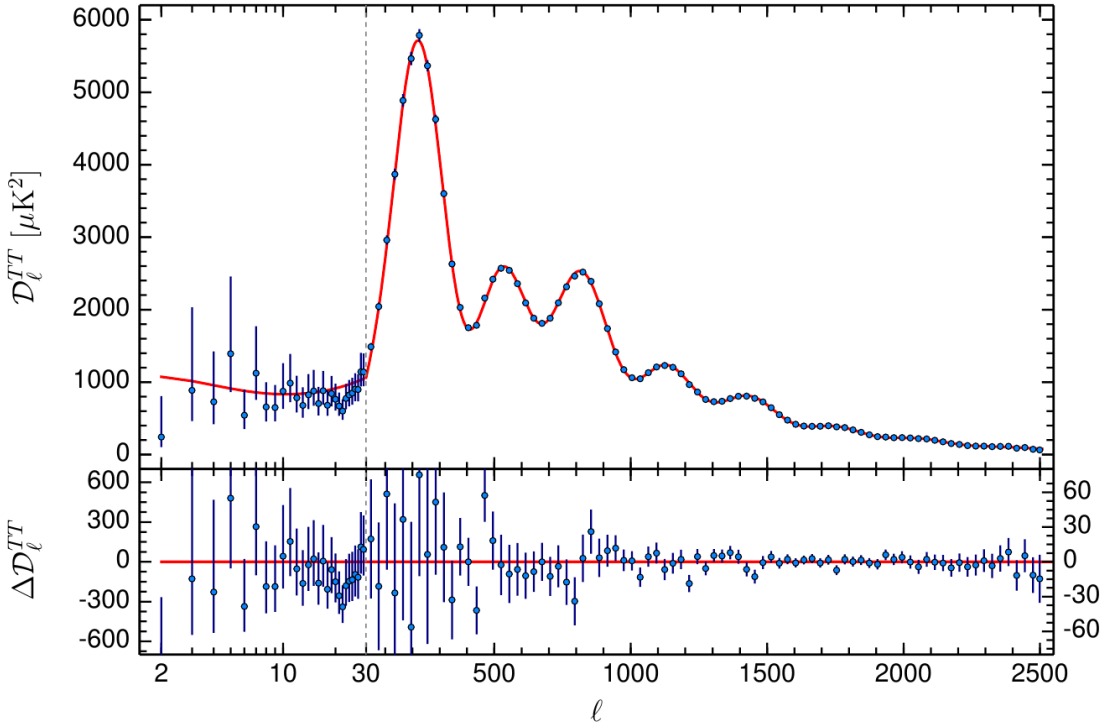

Figure 3.2: Planck 2015 temperature angular power spectrum [5] (blue circles with 1σ error bars) and the best-fit ΛCDM theoretical model (red line).

however measured only three decades later with the Cosmic Background Explorer (COBE)[6], published in 1992 [68] (Nobel prize 2006). In the following years several ground and balloon based experiments measured the first and tentatively the second acoustic peak, until the launch of the Wilkinson Microwave Anisotropy Probe (WMAP) in 2001 revealed the CMB angular power spectrum up to multipole order $\ell \sim 1000$ [69]. Finally, the Planck satellite (launched in 2009) measured the CMB angular power spectrum up to $\ell \sim 2500$, see figure 3.2. The first release of Planck data was in 2013 [70], followed by a next release in 2015 [5]. The final data release will presumably be in 2017. Even higher ℓ in the CMB angular power spectrum can be observed with ground based telescopes like e.g. the South Pole Telescope (SPT) [71, 72] or the Atacama Cosmology Telescope (ACT) [73, 74].

Comparing the measured angular power spectrum in figure 3.2 to our predictions from cosmic linear perturbation theory (3.52) allows us to derive constraints on the base parameters. Markov-Chain Monte-Carlo (MCMC) software packages like Cos-

[6]Shortly before, the Relikt-1 experiment [67] already announced the detection of a CMB quadrupole, however with much less precision than COBE.

moMC [7] [75] and Monte Python [76] explore the cosmological parameter space and reconstruct the posterior distribution for the free parameters. The CMB angular power spectrum is of course not only a powerful tool to constrain the six base parameters, but can also be used to constrain parameters describing various extensions of the ΛCDM model. Popular extensions are for example the effective number of relativistic degrees of freedom N_{eff} (more on this in chapter 6), the sum of neutrino masses $\sum m_\nu$, curvature Ω_{k} (1.11) and the equation of state of dark energy w.

[7] http://cosmologist.info/cosmomc

4 Reionization and dark matter decay

In the publication [1] attached to this chapter, we consider the impact of a decaying dark matter (DM) component on the angular power spectrum of the CMB. A DM component that decays into electromagnetically interacting daughter particles (e.g. photons or electrons) can impact the CMB by (partially) reionizing the Universe.

The general expected signal from reionization on the CMB angular power spectrum is relatively easy to understand: When propagating through space to us, the intensity of the CMB radiation gets damped by a factor of $e^{-\tau}$, with the optical depth τ being defined as (see equation (2.6) in [1])

$$\tau(t) = \int_t^{t_0} \mathrm{d}t \, n_\mathrm{e} \sigma_\mathrm{T}, \tag{4.1}$$

where n_e is the number density of free electrons and σ_T the Thomson scattering cross section. Hence, the temperature angular power spectrum of the CMB is damped by a factor of $e^{-2\tau}$. This argument however only holds at scales that are well below the Hubble horizon ($\mathcal{H} \equiv aH < k$) at the time of recombination, which translates roughly into $\ell \gtrsim 200$. Larger scales enter the horizon after recombination and are damped less.

The polarization angular power spectrum experiences the same suppression of $e^{-2\tau}$ at $\ell \gtrsim 200$, as it reflects mainly the temperature quadrupole.

At large scales, reionization moreover represents a source for polarization, which results in a very characteristic *reionization bump*. The largest scales are therefore in principle not only sensitive to the optical depth (4.1), but also to the reionization history. This can be understood within the line-of-sight approach [66], where the photon Boltzmann equation (3.19), including Thomson scattering, is integrated over conformal time. Partial integration then reveals how the multipoles $F_{\gamma,\ell}$ not only depend on the optical depth (4.1), but also on its first and second derivatives.

In this work, we consider two possible sources of reionization: A late-time ($z \sim 10$) reionization – caused by the appearance of the first astrophysical objects emitting radiation energetic enough to ionize the Universe – and a decaying DM component. While the first reionization source (referred to as *astrophysical reionization* in [1]) is conventionally modelled as a sudden step-like increase of the free electron fraction (*CAMB parametrization*, equation (2.1) in [1]), we also consider another astrophysical reion-

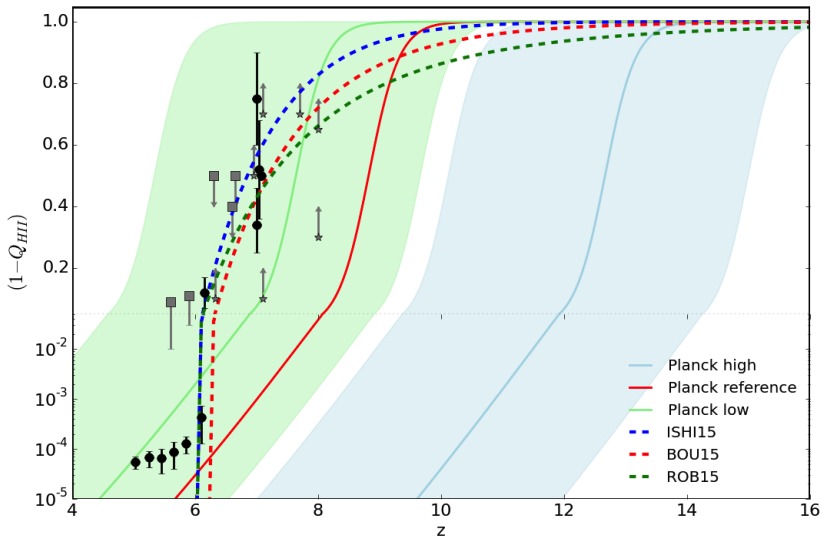

Figure 4.1: Filling factor of ionized hydrogen as a function of redshift z, figure taken from [77] with data points from [78].

ization scenario, which is motivated by direct observations of the free electron fraction [77–79] (*empirical parametrization*, equation (2.4) in [1]). Our study addresses the question of how strongly constraints on the DM decay rate from CMB data depend on the assumptions that we make about astrophysical reionization. We implement the new empirical parametrization in the Boltzmann code CAMB [65] and the impact of the decaying DM component on the reionization history in the recombination code CosmoRec [59, 60]. Based on this, we perform a Markov Chain Monte Carlo (MCMC) analysis of the Planck 2015 data [5] with the CosmoMC code [75] to derive constraints on the DM decay rate. Our analysis reveals that those constraints depend only very little on the chosen parametrization of astrophysical reionization. We therefore conclude that even though the details of the astrophysical reionization history are not yet well understood, we can still derive robust constraints on the DM decay rate. For a decaying DM component that decays exclusively into electromagnetically interacting particles we find for the decay rate $\Gamma < 5.3 \times 10^{-26}\mathrm{s}^{-1}$ at 95% CL within the so called on-the-spot approximation (see section 3.2.1 in [1]). We furthermore apply our results to a keV sterile neutrino as a specific decaying DM candidate, constraining thereby its mass and mixing angle.

Note that constraints on the decay rate of a DM component decaying only into the dark relativistic sector can also be obtained [80–82]. Such a scenario is naturally much weaker constrained, as its impact on the CMB angular power spectrum is a purely gravitational effect, i.e. $\Gamma < 2.0 \times 10^{-19}\mathrm{s}^{-1}$ [80] (assuming a single DM component).

Let us also briefly present the astrophysical observations that are the motivation for the empirical parametrization studied in this work [1] and first proposed in [77]. Figure 4.1 (taken from [77]) shows the filling factor of ionized hydrogen $Q_{HII} = n_{\rm HII}/n_{\rm H}$ as a function of redshift. The data points at $z \lesssim 6.5$ are derived from the spectra of quasars and the data points at higher redshifts are derived from star-forming galaxies (Lyman-α emitters), see references within [77,78]. The dashed curves are obtained by integration over the ionization rate as compiled in [79]. Blue and green bands show the CAMB parametrization for different values of the redshift of reionization $z_{\rm re}$. As obvious from figure 4.1, for any choice of $z_{\rm re}$ the CAMB parametrization is not a good fit to the direct observations of $Q_{\rm HII}$. This prompted the authors of [77] to propose the new empirical parametrization, where the filling factor $Q_{\rm HII}$ has an exponential dependence on z at high redshifts and a power-law dependence at low redshifts.

Publication JCAP 1608 (2016) no. 08, 054

The main work of the following publication was done by myself. I implemented the empirical parametrization in the CAMB code and the decaying DM component in the CosmoRec code. I also derived the main results in chapter 4 by performing the MCMC analysis. The main text was written by myself and edited by Dr. Daniel Boriero and Prof. Dominik J. Schwarz. Section 4.4 and parts of section 4.1 were however written by Dr. Daniel Boriero and edited by myself and Prof. Dominik Schwarz.

http://dx.doi.org/10.1088/1475-7516/2016/08/054

5 Interacting neutrinos in the cosmic microwave background

The following two publications deal with the effect of non-standard neutrino interactions on the angular power spectrum of the cosmic microwave background.

We consider theories in which neutrinos couple to a scalar particle via Yukawa coupling. Such neutrino interactions appear for example in majoron-like models that were first proposed in [83]. Majoron models provide a mechanism of neutrino mass generation and furthermore explain the smallness of neutrino masses similarly to the see-saw mechanism. In general, a Majorana-mass term for neutrinos is created by spontaneously broken $U(1)_{\text{B-L}}$ symmetry. This also implies the appearance of a new Goldstone boson, which is called the majoron and couples mainly to neutrinos. See [84] for a review.

The first publication [2] in section 5.1 is a mainly analytical study. The starting point is the perturbed collisional Boltzmann equation (3.19) for neutrinos. After calculating the collision integral (1.22) on the r.h.s. of the Boltzmann equation (3.19) for the new neutrino interactions, the Boltzmann hierarchy (3.33)-(3.35) for interacting neutrinos is derived. We thereby study the case of a very massive scalar (i.e. the scalar mass far exceeds the typical neutrino energy) and the case of an effectively massless scalar. In the massive scalar case, the coupling becomes effectively a Fermi-like interaction, with the scalar particle only playing the role of an exchange particle for neutrino self-interactions. The massless case however also necessitates the computation of a scalar Boltzmann hierarchy. The resulting neutrino and scalar Boltzmann hierarchies (equations (6.6), (6.13) and (6.15) in [2]) contain momentum-dependent collision terms and look formally very different to the approaches by others. This prompted us to continue our studies in a second publication.

The second publication [3] in section 5.2 splits into two parts: Firstly, the exact Boltzmann hierarchy for interacting neutrinos (equation (6.6) in [2] or (2.1) in [3]) is implemented in the Boltzmann code CLASS [64]. The resulting signal on the CMB angular power spectrum is compared to the approaches by others, i.e. the relaxation time approximation [85] (equation (2.7) in [3]) and the $(c^2_{\text{eff}}, c^2_{\text{vis}})$-parametrization [86] (equation (2.6) in [3]). The relaxation time approximation shows a very good agreement with our

exact approach, whereas the agreement with the widely used $(c^2_{\rm eff}, c^2_{\rm vis})$-parametrization is very poor. Secondly, we perform a MCMC analysis to derive constraints on the effective neutrino coupling $G_{\rm eff}$. Due to the remarkable agreement with the relaxation time approximation and in order to save computational resources, we perform our analysis by using this approximation. Interestingly, our analysis reveals two modes in the allowed cosmological parameter space, one mode in which neutrinos are effectively non-interacting and a second mode in which neutrinos are self-interacting with a coupling of $G_{\rm eff} \sim 3 \times 10^9\, G_{\rm F}$ (where $G_{\rm F}$ is the Fermi coupling).

5.1 Publication JCAP 1504 (2015) no. 04, 016

I have been the main contributor to the following publication. Parts of the analytical work were already derived during my master thesis with Prof. Yvonne Y. Y. Wong at RWTH Aachen (November 2011 - November 2012). To be precise, during my master thesis, I focussed on the case of a massless scalar with only neutrino self-interactions. During my doctoral studies, we extended this work by including the case of a massive scalar. We furthermore included annihilation processes $\nu\nu \leftrightarrow \phi\phi$ and scattering events $\nu\phi \leftrightarrow \nu\phi$ to the massless scalar case. All calculations have first been performed by myself and then revised and edited by Prof. Y. Y. Y. Wong and Dr. Cornelius Rampf. The main text of the publication was first written by myself and then edited by my collaborators.

http://dx.doi.org/10.1088/1475-7516/2015/04/016

5.2 Publication JCAP 1711 (2017) no. 11, 027

My contribution to the following publication was the implementation of the neutrino Boltzmann hierarchy in the Boltzmann code CLASS. The MCMC analysis in section 4 was performed by my collaborator Dr. Thomas Tram. The main text was first written by myself and edited by my collaborators. Section 4 was however written by Dr. Thomas Tram and edited by myself and our collaborators.

http://dx.doi.org/10.1088/1475-7516/2017/11/027

6 Improved constraints on lepton asymmetry from the cosmic microwave background

The publication attached to this chapter [4] deals with a potentially non-negligible lepton asymmetry in our Universe. Before summarizing this work, let us first explain the impact of lepton asymmetry on BBN and the CMB angular power spectrum in some more detail than it is done in the publication.

Lepton asymmetry is defined as the difference between the number densities of leptons and anti-leptons divided by the photon number density, i.e.

$$\eta_{\mathrm{l}} = \frac{n_{\mathrm{l}} - n_{\bar{\mathrm{l}}}}{n_\gamma}. \tag{6.1}$$

The charge neutrality of the Universe implies that the lepton asymmetry of charged leptons must be of the same order as the baryon asymmetry $\mathcal{O}(10^{-9})$ (2.4), i.e. negligibly small [87]. A lepton asymmetry – if existent – must therefore be carried by neutrinos and can be expressed by their chemical potentials $\xi_\alpha = \mu_\alpha / T_\nu$ (where α denotes the flavour), see equation (1) in [4]. The chemical potentials of neutrinos must be equal but with opposite sign to those of anti-neutrinos, i.e. $\xi_{\bar{\alpha}} = -\xi_\alpha$. This follows from the following argument [87]: Since photons can be emitted and absorbed in an arbitrary reaction, equation (1.26) (chemical equilibrium) shows that $\mu_\gamma = 0$. Furthermore, *charged* leptons and anti-leptons can annihilate into photons (e.g. $e^- + e^+ \leftrightarrow \gamma$) implying that $\mu_{\mathrm{l}^+} = -\mu_{\mathrm{l}^-}$. Since neutrinos and anti-neutrinos can annihilate into charged leptons and anti-leptons (e.g. $\nu + \bar{\nu} \leftrightarrow e^- + e^+$), we consequently find that $\mu_{\bar{\alpha}} = -\mu_\alpha$.

In this work, we focus on the impact of lepton asymmetry on the epochs of BBN and the formation of the CMB. The impact of lepton asymmetry on BBN is two-fold. First, lepton asymmetry enhances the energy density in the neutrino sector according to

$$\begin{aligned} \rho_{\nu,\bar{\nu}} &= \sum_{\alpha=e,\mu,\tau} \rho_{\nu_\alpha} + \rho_{\bar{\nu}_\alpha} = \sum_{\alpha=e,\mu,\tau} \int \frac{\mathrm{d}^3 p}{(2\pi)^3} p \left(\frac{1}{e^{p/T_{\nu_\alpha} - \xi_\alpha} + 1} + \frac{1}{e^{p/T_{\nu_\alpha} + \xi_\alpha} + 1} \right) \\ &= 2 \frac{7}{8} \frac{\pi^2}{30} \sum_{\alpha=e,\mu,\tau} T_{\nu_\alpha}^4 \left(1 + \frac{30}{7} \left(\frac{\xi_\alpha}{\pi} \right)^2 + \frac{15}{7} \left(\frac{\xi_\alpha}{\pi} \right)^4 \right), \end{aligned} \tag{6.2}$$

where we explicitly assumed zero neutrino masses. See [88] for a discussion of the massive neutrino case, which we are not studying in this work. An increased energy density of neutrinos can be expressed by an enhanced *number of relativistic degrees of freedom* N_{eff}, which is most generally defined as

$$\begin{aligned} \rho_{\text{rel}} = \rho_\gamma + \rho_\nu + \rho_{\text{DR}} &\equiv \left[1 + \frac{7}{8}\left(\frac{4}{11}\right)^{\frac{4}{3}} N_{\text{eff}}\right] \rho_\gamma \\ \implies N_{\text{eff}} &\equiv \frac{8}{7}\left(\frac{11}{4}\right)^{\frac{4}{3}} \frac{\rho_{\text{DR}}}{\rho_\gamma} + \left(\frac{11}{4}\right)^{\frac{4}{3}} \sum_\alpha \left(\frac{T_{\nu_\alpha}}{T_\gamma}\right)^4 \left[1 + \frac{30}{7}\left(\frac{\xi_\alpha}{\pi}\right)^2 + \frac{15}{7}\left(\frac{\xi_\alpha}{\pi}\right)^4\right]. \end{aligned} \tag{6.3}$$

Here, ρ_{DR} denotes the energy density of a hypothetical component of *dark radiation*, i.e. a species of relativistic particles other than neutrinos or photons. We however assume $\rho_{\text{DR}} = 0$ throughout this work.

As mentioned earlier, neutrinos decouple from photons and electrons at ~ 1 MeV. Shortly afterwards, electrons and positrons annihilate into photons, which transfers energy into the photon sector and enhances the photon temperature compared to the neutrino temperature. For standard neutrinos, the ratio of the neutrino to photon temperature follows from entropy conservation to be $T_{\nu_\alpha}/T_\gamma \approx (4/11)^{1/3}$, see e.g. [6–8]. For the case of three flavours of standard neutrinos with zero chemical potentials we therefore find $N_{\text{eff}} = 3.046$ [89], where the small correction to $N_{\text{eff}} = 3.0$ arises since high energetic neutrinos from the tail of the distribution get heated from $e^\pm$-annihilation.

From the definition (6.3) we see that in general N_{eff} can be altered by several contributions: a dark radiation component, a neutrino temperature different from $(4/11)^{1/3} T_\gamma$, a number of neutrino species different from 3, or the appearance of neutrino chemical potentials (i.e. lepton asymmetry). In this work, we only consider the last one, i.e. neutrino chemical potentials. Due to the only even powers of ξ_α in (6.3), neutrino chemical potentials always *increase* N_{eff}, which leads to an earlier freeze-out of weak interactions (2.1) and in turn decreases the neutron-to-proton ratio (2.3) at the onset of BBN.

The second effect of lepton asymmetry on BBN is a change of the weak reaction processes (2.1)-(2.2) that regulate the neutron-to-proton ratio. In contrast to the modified effective number of relativistic degrees of freedom (6.3), this effect only depends on the chemical potential of electron neutrinos. The $n \to p$ weak reaction rate is calculated according to [29, 90]

$$\begin{aligned} \lambda_{n\to p} = K \int_1^\infty \mathrm{d}x \frac{x(x+q)^2(x^2-1)^{1/2}}{(1+e^{-xz})[1+e^{(x+q)z_\nu+\xi_{\text{e}}}]} \\ + K \int_1^\infty \mathrm{d}x \frac{x(x-q)^2(x^2-1)^{1/2}}{(1+e^{xz})[1+e^{-(x-q)z_\nu+\xi_{\text{e}}}]}, \end{aligned} \tag{6.4}$$

where $q = (m_\mathrm{n} - m_\mathrm{p})/m_\mathrm{e}$, $z = m_\mathrm{e}/T_\gamma$ and $z_\nu = m_\mathrm{e}/T_\nu$. The normalization constant K is fixed by demanding that the rate (6.4) matches the free neutron decay rate at low temperatures, i.e. $\lambda_{n\to p} \to 1/\tau_\mathrm{n}$ for $z \gg 1$. The inverse reaction rate ($p \to n$) is simply given by $\lambda_{n\to p}(-q, -\xi_\mathrm{e})$. In equilibrium, the neutron-to-proton ratio (2.3) is roughly altered by a factor of $e^{-\xi_\mathrm{e}}$ [90], i.e. a positive chemical potential reduces the neutron-to-proton ratio. Both of these effects – the enhanced N_eff (6.3) and the modified weak processes (6.4) – alter the BBN predictions for the primordial abundances of helium and other light elements.

Finally, the CMB angular power spectrum is also altered in presence of a lepton asymmetry in two ways: An increased N_eff (6.3) delays the time of matter-radiation equality. This enhances the first acoustic peak in the CMB angular power spectrum (figure 3.2) and the position of the subsequent other peaks. This effect is generally referred to as *early Intgrated Sachs-Wolfe* (ISW) effect [91], see also e.g. [8,10]. Furthermore, a modified value of the primordial helium abundance alters the angular power spectrum on small scales, i.e. at large ℓ in the so called *damping tail*. This can be understood in the following way: Thomson scattering between photons and electrons has a finite mean free path. For large scales (small ℓ) this mean free path is effectively negligible, but for small scales (large ℓ) the mean free path becomes significant and anisotropies are washed out below the so called *Silk scale* [92]. This is also the reason why the CMB angular power spectrum in figure 3.2 is damped at $\ell \gtrsim 1000$ and is generally referred to as *diffusion damping*. On small scales, an enhanced amount of helium implies less free electrons (at hydrogen recombination time), a larger diffusion length and therefore more diffusion damping at those scales.

In this work, we perform an MCMC analysis of the Planck 2015 data [5] to derive constraints on the lepton asymmetry of the Universe. In order to impose BBN consistency we produced a table for the helium abundance Y_p as a function of ω_b and ξ with the BBN code AlterBBN [31], assuming thereby equal flavour asymmetries ($\xi_\mathrm{e} = \xi_\mu = \xi_\tau$). We implemented the modified helium amount $Y_\mathrm{p}(\omega_\mathrm{b}, \xi)$ together with the modified effective number of relativistic degrees of freedom $N_\mathrm{eff}(\xi)$ (6.3) in the Boltzmann code CLASS [64] and performed an MCMC analysis with the MCMC engine Monte Python [76]. We find $\xi = -0.002^{+0.114}_{-0.111}$ (95% CL) for the chemical potentials, implying that $-0.085 \leq \eta_\mathrm{l} \leq 0.084$. Note that even though we implemented our analysis in a BBN consistent way, our constraints are obtained from CMB data alone and are independent of direct measurements of primordial abundances of light elements. Our constraints are significantly stronger than previous constraints on lepton asymmetry from CMB data [93–97] and we argue that they are more robust than those from direct observations of primordial light element abundances [40,98,99].

Let us shortly also comment on the assumption of equal flavour asymmetries. In

general, the initial flavour asymmetries could have different values, but neutrino oscillations are likely to equilibrate flavour asymmetries before the onset of BBN [100, 101]. This however does not hold generically, but depends in detail on the values of the mixing angle as well as on the initial values of the flavour asymmetries [99, 102, 103]. This also implies that the relation between $\eta_{\mathrm{l}}(\xi_\alpha)$ in equation (1) in [4] and $N_{\mathrm{eff}}(\xi_\alpha)$ in equation (2) in [4] does not necessarily hold any more [104].

Publication Europhys. Lett. 119 (2017) no. 2, 29001

I have been the main contributor in producing the results of the following publication. The text was written by myself and afterwards edited by my advisor Prof. D. J. Schwarz.

http://dx.doi.org/10.1209/0295-5075/119/29001

7 Conclusions

In this thesis, we have studied and constrained the impact of different particle properties on the angular power spectrum of the cosmic microwave background. The content and results of this thesis can be divided into three major topics, namely: i) the impact of a decaying dark matter component on the reionization history of the Universe in chapter 4, ii) the impact of non-standard neutrino interactions on the CMB in 5, and iii) constraints on lepton asymmetry from CMB data in chapter 6.

In the work presented in chapter 4 and published in [1], we considered a decaying dark matter component as an additional source of reionization to the astrophysical reionization process. To model the astrophysical reionization process we used two different parametrizations, the conventional parametrization used by the CAMB code (CAMB parametrization, equation (2.1) in [1]) and the empirically motivated parametrization proposed by [77] (empirical parametrization, equation (2.4) in [1]). We implemented the empirical parametrization in the CAMB code and the impact of dark matter decay on reionization into the recombination code CosmoRec. The latter one required furthermore the implementation of additional effects that are not included in the Recfast++ runmode of CosmoRec, namely a correction of the photon ionization coefficient and collisional ionizations.

We performed an MCMC analysis to derive constraints on the effective dark matter decay rate Γ_{eff} using the Planck 2015 data [5]. We found $\Gamma_{\text{eff}} < 2.6 \times 10^{-25} s^{-1}$ using the CAMB parametrization and $\Gamma_{\text{eff}} < 2.9 \times 10^{-25} s^{-1}$ using the empirical parametrization at 95 % CL, i.e. the constraints agree within 10 %. We conclude that the constraints on Γ_{eff} are relatively independent of the choice for the parametrization for astrophysical reionization. Our constraints were obtained within the on-the-spot approximation, which strictly speaking overestimates the impact of dark matter decay on reionization. More realistic constraints are expected to be weaker, but are also dependent on the details of the specific dark matter decay model. Going beyond the on-the-spot approximation, we also applied our work to one specific dark matter candidate, i.e. a keV-mass sterile neutrino that has been claimed to be detected at 3.5 keV [105, 106]. The constraints on the decay rate were translated into constraints on the mass m_{s} and the mixing angle θ of the sterile neutrino. The 3.5 keV sterile neutrino as a single dark matter component seems however to be almost ruled out by recent observations of X-ray data, the

Lyman-α forest and subhalo counts, e.g. [107, 108].

In the work presented in chapter 5 and published in [2, 3], we studied a scenario in which neutrinos are coupled to new scalar particles via Yukawa coupling.

In section 5.1 [2], we computed for the first time and from first principles the neutrino and scalar Boltzmann hierarchies including neutrino–neutrino and neutrino–scalar interactions up to first order in space-time perturbations. We thereby focussed on two limiting cases of the scalar mass, i.e. the case of an effectively massless scalar and the case of a very massive scalar (where the scalar mass far exceeds the neutrino energies at all times of interest). In the massive scalar case, the population of the scalar particle is thermally suppressed and the interaction becomes effectively a four-fermion interaction, with the massive scalar serving only as a mediator particle. For the massless scalar case, the scalar particle can be produced, which demands to track also the neutrino and scalar background populations. We therefore also derived the zeroth-order Boltzmann equation for this case.

In contrast to various heuristic models of neutrino interactions in the literature, our findings for the neutrino and scalar Boltzmann hierarchies (equations (6.6) and (6.13) in [2]) reveal a much richer structure of the collision terms, as they show a momentum dependence that reflects significant energy transfer in neutrino–neutrino scattering (and neutrino–scalar scattering).

Based on these results, we investigated the phenomenology of non-standard neutrino interactions on the CMB angular power spectrum in a subsequent publication [3]. We thereby focussed on the massive scalar case only. We implemented the exact Boltzmann hierarchy for interacting neutrinos (found in our previous work [2]) into the Boltzmann solver CLASS. We compared our exact approach with two other approaches used in the literature: the "separable ansatz" or relaxation time approximation (RTA), first introduced in [85], and the popular $\left(c^2_{\text{eff}}, c^2_{\text{vis}}\right)$-parametrization.

The agreement between our exact approach and the RTA is very good – at the level of the neutrino fluid perturbations (i.e. energy contrast, velocity divergence etc.) as well as at the level of the CMB angular power spectrum. The agreement to the widely used $\left(c^2_{\text{eff}}, c^2_{\text{vis}}\right)$-parametrization is however very poor. We therefore conclude that this parametrization has no interpretation in terms of neutrino scattering and should not be used in order to describe non-standard neutrino physics in future works.

Using the RTA we furthermore derived constraints on the effective neutrino coupling G_{eff}. We performed an MCMC analysis using Planck 2015 temperature and polarization data [5], local measurements of the Hubble constant [109] and BOSS baryonic oscillation data [110–113]. Remarkably, all combinations of datasets reveal two separated modes in the posterior distributions of the cosmological parameters. While one mode presents an effectively free-streaming neutrinos scenario, the other mode

presents a scenario in which neutrino self-interact with an effective coupling constant $G_{\rm eff} \simeq 0.03\,\mathrm{MeV}^{-2} \simeq 3 \times 10^9\,G_{\rm F}$, where $G_{\rm F}$ is the Fermi coupling. The interacting mode is accompanied by a reduced spectral index $n_{\rm s}$, which could have interesting consequences for inflation. Another interesting feature of the interacting mode is an increase of the inferred value for the Hubble constant H_0, which weakens but not resolves the tension to local measurements of the Hubble constant. Shortly before completion of this work, the preprint [114] appeared, which also presents cosmological constraints on neutrino self-interactions and comes to similar conclusions like the ones obtained in our work.

In the work presented in chapter 6 and published in [4], we considered the impact of a non-negligible lepton asymmetry on the CMB angular power spectrum. We thereby assumed negligible neutrino masses and equal flavour asymmetries. Using the AlterBBN code, we produced a table for the helium fraction $Y_{\rm p}$ as a function of the baryon density $\omega_{\rm b}$ and the unitless neutrino chemical potential ξ. Furthermore, we modified the CLASS code to account for the increased number of relativistic degrees of freedom $N_{\rm eff}(\xi)$ and the modified helium amount $Y_{\rm p}(\omega_{\rm b}, \xi)$.

We performed an MCMC analysis to derive constraints on the dimensionless neutrino chemical potentials using the Planck 2015 data [5]. We found $\xi = -0.002^{+0.114}_{-0.111}$ (95% CL) from the high-ℓ and low-ℓ temperature and polarization data and lensing reconstruction, which implies $-0.085 \leq \eta_{\rm l} \leq 0.084$ (95% CL) for the lepton asymmetry. Our constraints are significantly stronger than previous constraints from CMB data [93–95, 97]. They are weaker (factor ~ 2) than the constraints obtained from direct measurements of light element abundances [93, 94, 97], but we argue that they are more robust, as direct measurements of primordial light elements still suffer from sizeable systematic uncertainties. Furthermore, our derived constraints on the primordial helium and deuterium abundance are in good agreement with direct measurements [39, 40].

To sum up, this thesis demonstrated – on the examples of dark matter decay, neutrino interactions and lepton asymmetry – that observations of the CMB have a large potential to constrain physics beyond the Standard Model. In a future work, an interesting direction to follow would be a study of the quantum-kinetic equations (density matrix formalism, see e.g. [115] or [7] for a review), which allow a simultaneous study of neutrino oscillations and neutrino interactions. A closer look into this is for example important in order to extend our analysis in [4] to the case of initially different flavour asymmetries and also to include neutrino masses. In the same manner, it would also be interesting to study how the non-standard neutrino interactions studied in [2, 3] would change the neutrino spectra at the times of weak decoupling and the onset of neutrino oscillations.

Acknowledgements

First of all, I would like to thank Prof. Dominik J. Schwarz for supervising me during the last years. I thank him for not only teaching me various things about cosmology, but also for sending me to many schools and conferences and for supporting me to follow my own research ideas.

I also thank the second referee Prof. Nicolas Borghini for evaluating this thesis and the other members of the committee for their participation in the disputation process.

I am thankful to my collaborators Cornelius Rampf, Daniel Boriero, Thomas Tram and Yvonne Wong for fruitful discussions and great collaborations.

I thank all members of the group of Prof. Schwarz for interesting group meetings and discussions, in particular Daniel Boriero, Matthias Rubart, Patric Hölscher, Samae Bagheri, Song Chen and Thilo Siewert. Also many thanks to Giuseppe Gagliardi, Mandy Wygas and Song Chen for being so nice office maids, and to Daniel Boriero and Thomas Luthe for proof-reading this thesis. I am also thankful to Gudrun Eickmeyer and Susi v. Reder for helping me with many administrative things during the last years.

I thank The Physics Gang in Bielefeld for filling the last years with many great memories: Daniel Boriero, Florian Meyer, Samae Bagheri, Song Chen and Thomas Luthe.

Special thanks to my husband Jan for having listened to many long monologues about my work and cosmology and never giving up to teach me about basic chemistry. I thank my parents, my brother and my grandmother for always supporting me.

I gratefully acknowledge the financial support and the organization of interesting interdisciplinary PhD meetings by Studienstiftung des Deutschen Volkes. I am also thankful to the research training group "Models of Gravity" for interesting colloquia and travel support.

Bibliography

[1] I. M. Oldengott, D. Boriero, and D. J. Schwarz, "Reionization and dark matter decay," JCAP **1608** (2016) no. 08, 054, arXiv:1605.03928 [astro-ph.CO].

[2] I. M. Oldengott, C. Rampf, and Y. Y. Y. Wong, "Boltzmann hierarchy for interacting neutrinos I: formalism," JCAP **1504** (2015) no. 04, 016, arXiv:1409.1577 [astro-ph.CO].

[3] I. M. Oldengott, T. Tram, C. Rampf, and Y. Y. Y. Wong, "Interacting neutrinos in cosmology: Exact description and constraints," JCAP **1711** (2017) no. 11, 027, arXiv:1706.02123 [astro-ph.CO].

[4] I. M. Oldengott and D. J. Schwarz, "Improved constraints on lepton asymmetry from the cosmic microwave background," Europhys. Lett. **119** (2017) no. 2, 29001, arXiv:1706.01705 [astro-ph.CO].

[5] **Planck** Collaboration, P. A. R. Ade et al., "Planck 2015 results. XIII. Cosmological parameters," arXiv:1502.01589 [astro-ph.CO].

[6] E. W. Kolb and M. S. Turner, The Early Universe. Addison-Wesley Publishing Company, 1989.

[7] J. Lesgourgues, G. Mangano, G. Miele, and S. Pastor, Neutrino Cosmology. Cambridge University Press, 2013.

[8] S. Dodelson, Modern Cosmology. Elsevier, 2003.

[9] V. Mukhanov, Physical Foundations of Cosmology. Cambridge University Press, 2005.

[10] R. Durrer, The Cosmic Microwave Background. Cambridge University Press, 2008.

[11] E. Hubble, "A Relation between Distance and Radial Velocity among Extra-Galactic Nebulae,"Proceedings of the National Academy of Science **15** (Mar., 1929) 168–173.

[12] **HST** Collaboration, W. L. Freedman et al., "Final results from the Hubble Space Telescope key project to measure the Hubble constant," Astrophys. J. **553** (2001) 47–72, arXiv:astro-ph/0012376 [astro-ph].

[13] J. Bernstein, KINETIC THEORY IN THE EXPANDING UNIVERSE. Cambridge University Press, Cambridge, U.K., 1988.

[14] K. Huang, Statistical Mechanics. John Wiley & Sons, 1987.

[15] A. A. Starobinsky, "Spectrum of relict gravitational radiation and the early state of the universe," JETP Lett. **30** (1979) 682–685. [Pisma Zh. Eksp. Teor. Fiz.30,719(1979)].

[16] A. H. Guth, "The Inflationary Universe: A Possible Solution to the Horizon and Flatness Problems," Phys. Rev. **D23** (1981) 347–356.

[17] V. C. Rubin and W. K. Ford, Jr., "Rotation of the Andromeda Nebula from a Spectroscopic Survey of Emission Regions," Astrophys. J. **159** (1970) 379–403.

[18] V. C. Rubin, N. Thonnard, and W. K. Ford, Jr., "Rotational properties of 21 SC galaxies with a large range of luminosities and radii, from NGC 4605 /R = 4kpc/ to UGC 2885 /R = 122 kpc/," Astrophys. J. **238** (1980) 471.

[19] A. Refregier, "Weak gravitational lensing by large scale structure," Ann. Rev. Astron. Astrophys. **41** (2003) 645–668, arXiv:astro-ph/0307212 [astro-ph].

[20] J. A. Tyson, G. P. Kochanski, and I. P. Dell'Antonio, "Detailed mass map of CL0024+1654 from strong lensing," Astrophys. J. **498** (1998) L107, arXiv:astro-ph/9801193 [astro-ph].

[21] **WMAP** Collaboration, E. Komatsu et al., "Seven-Year Wilkinson Microwave Anisotropy Probe (WMAP) Observations: Cosmological Interpretation," Astrophys. J. Suppl. **192** (2011) 18, arXiv:1001.4538 [astro-ph.CO].

[22] **Supernova Cosmology Project** Collaboration, S. Perlmutter et al., "Measurements of the cosmological parameters Omega and Lambda from the first 7 supernovae at z>=0.35," Astrophys. J. **483** (1997) 565, arXiv:astro-ph/9608192 [astro-ph].

[23] **Supernova Search Team** Collaboration, A. G. Riess et al., "Observational evidence from supernovae for an accelerating universe and a cosmological constant," Astron. J. **116** (1998) 1009–1038, arXiv:astro-ph/9805201 [astro-ph].

[24] S. M. Carroll, "The Cosmological constant," Living Rev. Rel. **4** (2001) 1, arXiv:astro-ph/0004075 [astro-ph].

[25] G. Steigman, "Primordial nucleosynthesis: successes and challenges," Int. J. Mod. Phys. **E15** (2006) 1–36, arXiv:astro-ph/0511534 [astro-ph].

[26] G. Steigman, "Primordial Nucleosynthesis in the Precision Cosmology Era," Ann. Rev. Nucl. Part. Sci. **57** (2007) 463–491, arXiv:0712.1100 [astro-ph].

[27] **Particle Data Group** Collaboration, K. A. Olive et al., "Review of Particle Physics," Chin. Phys. **C38** (2014) 090001.

[28] A. Coc, J.-P. Uzan, and E. Vangioni, "Standard big bang nucleosynthesis and primordial CNO Abundances after Planck," JCAP **1410** (2014) 050, arXiv:1403.6694 [astro-ph.CO].

[29] L. Kawano, "Let's go: Early universe. 2. Primordial nucleosynthesis: The Computer way,".

[30] O. Pisanti, A. Cirillo, S. Esposito, F. Iocco, G. Mangano, et al., "PArthENoPE: Public Algorithm Evaluating the Nucleosynthesis of Primordial Elements," Comput.Phys.Commun. **178** (2008) 956–971, arXiv:0705.0290 [astro-ph].

[31] A. Arbey, "AlterBBN: A program for calculating the BBN abundances of the elements in alternative cosmologies," Comput. Phys. Commun. **183** (2012) 1822–1831, arXiv:1106.1363 [astro-ph.CO].

[32] R. V. Wagoner, W. A. Fowler, and F. Hoyle, "On the Synthesis of elements at very high temperatures," Astrophys.J. **148** (1967) 3–49.

[33] P. D. Serpico, S. Esposito, F. Iocco, G. Mangano, G. Miele, and O. Pisanti, "Nuclear reaction network for primordial nucleosynthesis: A Detailed analysis of rates, uncertainties and light nuclei yields," JCAP **0412** (2004) 010, arXiv:astro-ph/0408076 [astro-ph].

[34] A. T. Yue, M. S. Dewey, D. M. Gilliam, G. L. Greene, A. B. Laptev, J. S. Nico, W. M. Snow, and F. E. Wietfeldt, "Improved Determination of the Neutron Lifetime," Phys. Rev. Lett. **111** (2013) no. 22, 222501, arXiv:1309.2623 [nucl-ex].

[35] R. N. Boyd, C. R. Brune, G. M. Fuller, and C. J. Smith, "New Nuclear Physics for Big Bang Nucleosynthesis," Phys.Rev. **D82** (2010) 105005, arXiv:1008.0848 [astro-ph.CO].

[36] V. Voronchev, Y. Nakao, and M. Nakamura, "Non-thermal processes in standard big bang nucleosynthesis. I: In-flight nuclear reactions induced by energetic protons," JCAP **0805** (2008) 010.

[37] Y. Nakao, K. Tsukida, and V. T. Voronchev, "Realistic neutron energy spectrum and a possible enhancement of reaction rates in the early Universe plasma," Phys.Rev. **D84** (2011) 063016.

[38] A. Coc, "Primordial Nucleosynthesis," 2016. arXiv:1609.06048 [astro-ph.CO]. http://inspirehep.net/record/1487411/files/arXiv:1609.06048.pdf.

[39] E. Aver, K. A. Olive, and E. D. Skillman, "The effects of He I λ10830 on helium abundance determinations," JCAP **1507** (2015) no. 07, 011, arXiv:1503.08146 [astro-ph.CO].

[40] R. Cooke, M. Pettini, R. A. Jorgenson, M. T. Murphy, and C. C. Steidel, "Precision measures of the primordial abundance of deuterium," Astrophys. J. **781** (2014) no. 1, 31, arXiv:1308.3240 [astro-ph.CO].

[41] T. M. Bania, R. T. Rood, and D. S. Balser, "The cosmological density of baryons from observations of 3He+ in the Milky Way," Nature **415** (2002) 54–57.

[42] M. Pettini and R. Cooke, "A new, precise measurement of the primordial abundance of Deuterium," Mon. Not. Roy. Astron. Soc. **425** (2012) 2477–2486, arXiv:1205.3785 [astro-ph.CO].

[43] L. Sbordone et al., "The metal-poor end of the Spite plateau. 1: Stellar parameters, metallicities and lithium abundances," Astron. Astrophys. **522** (2010) A26, arXiv:1003.4510 [astro-ph.GA].

[44] B. D. Fields, "The primordial lithium problem," Ann.Rev.Nucl.Part.Sci. **61** (2011) 47–68, arXiv:1203.3551 [astro-ph.CO].

[45] M. Asplund, D. L. Lambert, P. E. Nissen, F. Primas, and V. V. Smith, "Lithium isotopic abundances in metal-poor halo stars," Astrophys. J. **644** (2006) 229–259, arXiv:astro-ph/0510636 [astro-ph].

[46] F. Hammache et al., "High-energy break-up of 6Li as a tool to study the Big-Bang nucleosynthesis reaction 2H(alpha,gamma)6Li," Phys. Rev. **C82** (2010) 065803, arXiv:1011.6179 [nucl-ex].

[47] K. Lind, J. Melendez, M. Asplund, R. Collet, and Z. Magic, "The lithium isotopic ratio in very metal-poor stars," Astron. Astrophys. **554** (2013) A96, arXiv:1305.6564 [astro-ph.SR].

[48] M. Steffen, R. Cayrel, E. Caffau, P. Bonifacio, H. G. Ludwig, and M. Spite, "6Li detection in metal-poor stars: can 3D model atmospheres solve the second lithium problem?," Mem. Soc. Astron. Ital. Suppl. **22** (2012) 152, arXiv:1206.2239 [astro-ph.SR].

[49] D. J. Fixsen, "The Temperature of the Cosmic Microwave Background," Astrophys. J. **707** (2009) 916–920, arXiv:0911.1955 [astro-ph.CO].

[50] V. F. Mukhanov and G. V. Chibisov, "Quantum Fluctuations and a Nonsingular Universe," JETP Lett. **33** (1981) 532–535. [Pisma Zh. Eksp. Teor. Fiz.33,549(1981)].

[51] A. H. Guth and S. Y. Pi, "Fluctuations in the New Inflationary Universe," Phys. Rev. Lett. **49** (1982) 1110–1113.

[52] S. W. Hawking, "The Development of Irregularities in a Single Bubble Inflationary Universe," Phys. Lett. **B115** (1982) 295.

[53] A. A. Starobinsky, "Dynamics of Phase Transition in the New Inflationary Universe Scenario and Generation of Perturbations," Phys. Lett. **B117** (1982) 175–178.

[54] J. M. Bardeen, P. J. Steinhardt, and M. S. Turner, "Spontaneous Creation of Almost Scale - Free Density Perturbations in an Inflationary Universe," Phys. Rev. **D28** (1983) 679.

[55] R. H. Brandenberger, R. Kahn, and W. H. Press, "Cosmological Perturbations in the Early Universe," Phys. Rev. **D28** (1983) 1809.

[56] S. Seager, D. D. Sasselov, and D. Scott, "A new calculation of the recombination epoch," Astrophys. J. **523** (1999) L1–L5, arXiv:astro-ph/9909275 [astro-ph].

[57] P. J. E. Peebles, "Recombination of the Primeval Plasma," Astrophys. J. **153** (1968) 1.

[58] Ya. B. Zeldovich, V. G. Kurt, and R. A. Sunyaev, "Recombination of hydrogen in the hot model of the universe," Sov. Phys. JETP **28** (1969) 146. [Zh. Eksp. Teor. Fiz.55,278(1968)].

[59] J. Chluba and R. A. Sunyaev, "Induced two-photon decay of the 2s level and the rate of cosmological hydrogen recombination," Astron. Astrophys. **446** (2006) 39–42, arXiv:astro-ph/0508144 [astro-ph].

[60] J. Chluba and R. M. Thomas, "Towards a complete treatment of the cosmological recombination problem," Mon. Not. Roy. Astron. Soc. **412** (2011) 748, arXiv:1010.3631 [astro-ph.CO].

[61] Y. Ali-Haimoud and C. M. Hirata, "HyRec: A fast and highly accurate primordial hydrogen and helium recombination code," Phys. Rev. **D83** (2011) 043513, arXiv:1011.3758 [astro-ph.CO].

[62] C.-P. Ma and E. Bertschinger, "Cosmological perturbation theory in the synchronous and conformal Newtonian gauges," Astrophys. J. **455** (1995) 7–25, arXiv:astro-ph/9506072 [astro-ph].

[63] K. M. Gorski, E. Hivon, A. J. Banday, B. D. Wandelt, F. K. Hansen, M. Reinecke, and M. Bartelman, "HEALPix - A Framework for high resolution discretization, and fast analysis of data distributed on the sphere," Astrophys. J. **622** (2005) 759–771, arXiv:astro-ph/0409513 [astro-ph].

[64] D. Blas, J. Lesgourgues, and T. Tram, "The Cosmic Linear Anisotropy Solving System (CLASS) II: Approximation schemes," JCAP **1107** (2011) 034, arXiv:1104.2933 [astro-ph.CO].

[65] A. Lewis, "CAMB Notes." http://cosmologist.info/notes/CAMB.pdf.

[66] U. Seljak and M. Zaldarriaga, "A Line of sight integration approach to cosmic microwave background anisotropies," Astrophys. J. **469** (1996) 437–444, arXiv:astro-ph/9603033 [astro-ph].

[67] I. A. Strukov, A. A. Brukhanov, D. P. Skulachev, and M. V. Sazhin, "Anisotropy of the microwave background radiation," Soviet Astronomy Letters **18** (1992) 153.

[68] **COBE** Collaboration, G. F. Smoot et al., "Structure in the COBE differential microwave radiometer first year maps," Astrophys. J. **396** (1992) L1–L5.

[69] **WMAP** Collaboration, G. Hinshaw et al., "First year Wilkinson Microwave Anisotropy Probe (WMAP) observations: The Angular power spectrum," Astrophys. J. Suppl. **148** (2003) 135, arXiv:astro-ph/0302217 [astro-ph].

[70] **Planck** Collaboration, P. A. R. Ade et al., "Planck 2013 results. XVI. Cosmological parameters," Astron. Astrophys. **571** (2014) A16, arXiv:1303.5076 [astro-ph.CO].

[71] C. L. Reichardt et al., "A measurement of secondary cosmic microwave background anisotropies with two years of South Pole Telescope observations," Astrophys. J. **755** (2012) 70, arXiv:1111.0932 [astro-ph.CO].

[72] E. M. George et al., "A measurement of secondary cosmic microwave background anisotropies from the 2500-square-degree SPT-SZ survey," Astrophys. J. **799** (2015) no. 2, 177, arXiv:1408.3161 [astro-ph.CO].

[73] **ACT** Collaboration, J. W. Fowler et al., "The Atacama Cosmology Telescope: A Measurement of the 600< ell <8000 Cosmic Microwave Background Power Spectrum at 148 GHz," Astrophys. J. **722** (2010) 1148–1161, arXiv:1001.2934 [astro-ph.CO].

[74] S. Das et al., "The Atacama Cosmology Telescope: temperature and gravitational lensing power spectrum measurements from three seasons of data," JCAP **1404** (2014) 014, arXiv:1301.1037 [astro-ph.CO].

[75] A. Lewis and S. Bridle, "Cosmological parameters from CMB and other data: A Monte Carlo approach," Phys. Rev. **D66** (2002) 103511, arXiv:astro-ph/0205436 [astro-ph].

[76] B. Audren, J. Lesgourgues, K. Benabed, and S. Prunet, "Conservative Constraints on Early Cosmology: an illustration of the Monte Python cosmological parameter inference code," JCAP **1302** (2013) 001, arXiv:1210.7183 [astro-ph.CO].

[77] M. Douspis, N. Aghanim, S. Ilić, and M. Langer, "A new parameterization of the reionisation history," Astron. Astrophys. **580** (2015) L4, arXiv:1509.02785 [astro-ph.CO].

[78] R. J. Bouwens, G. D. Illingworth, P. A. Oesch, J. Caruana, B. Holwerda, R. Smit, and S. Wilkins, "Reionization after Planck: The Derived Growth of the Cosmic Ionizing Emissivity now matches the Growth of the Galaxy UV Luminosity Density," Astrophys. J. **811** (2015) no. 2, 140, arXiv:1503.08228 [astro-ph.CO].

[79] B. E. Robertson et al., "New Constraints on Cosmic Reionization from the 2012 Hubble Ultra Deep Field Campaign," Astrophys. J. **768** (2013) 71, arXiv:1301.1228 [astro-ph.CO].

[80] V. Poulin, P. D. Serpico, and J. Lesgourgues, "A fresh look at linear cosmological constraints on a decaying dark matter component," JCAP **1608** (2016) no. 08, 036, arXiv:1606.02073 [astro-ph.CO].

[81] B. Audren, J. Lesgourgues, G. Mangano, P. D. Serpico, and T. Tram, "Strongest model-independent bound on the lifetime of Dark Matter," JCAP **1412** (2014) no. 12, 028, arXiv:1407.2418 [astro-ph.CO].

[82] M. Lattanzi, S. Riemer-Sorensen, M. Tortola, and J. W. F. Valle, "Updated CMB and x- and γ-ray constraints on Majoron dark matter," Phys. Rev. **D88** (2013) no. 6, 063528, arXiv:1303.4685 [astro-ph.HE].

[83] Y. Chikashige, R. N. Mohapatra, and R. D. Peccei, "Are There Real Goldstone Bosons Associated with Broken Lepton Number?," Phys. Lett. **B98** (1981) 265–268.

[84] R. N. Mohapatra and P. B. Pal, Massive Neutrinos in Physics and Astrophysics. World Scientific Publishing Co. Pte. Ld., 2004.

[85] F.-Y. Cyr-Racine and K. Sigurdson, "Limits on Neutrino-Neutrino Scattering in the Early Universe," Phys. Rev. **D90** (2014) no. 12, 123533, arXiv:1306.1536 [astro-ph.CO].

[86] M. Archidiacono, E. Calabrese, and A. Melchiorri, "The Case for Dark Radiation," Phys. Rev. **D84** (2011) 123008, arXiv:1109.2767 [astro-ph.CO].

[87] S. Weinberg, Gravitation and Cosmology: Principles and Applications of the General Theory of Relativity. Wiley, New York [et al.], 1972.

[88] J. Lesgourgues and S. Pastor, "Cosmological implications of a relic neutrino asymmetry," Phys. Rev. **D60** (1999) 103521, arXiv:hep-ph/9904411 [hep-ph].

[89] G. Mangano, G. Miele, S. Pastor, T. Pinto, O. Pisanti, and P. D. Serpico, "Relic neutrino decoupling including flavor oscillations," Nucl. Phys. **B729** (2005) 221–234, arXiv:hep-ph/0506164 [hep-ph].

[90] G. Beaudet and P. Goret, "Leptonic Numbers and the Neutron to Proton Ratio in the Hot Bing Bang Model," Astron. Astrophys. **49** (1976) 415.

[91] R. K. Sachs and A. M. Wolfe, "Perturbations of a cosmological model and angular variations of the microwave background," Astrophys. J. **147** (1967) 73–90. [Gen. Rel. Grav.39,1929(2007)].

[92] J. Silk, "Cosmic black body radiation and galaxy formation," Astrophys. J. **151** (1968) 459–471.

[93] L. A. Popa and A. Vasile, "WMAP 5-year constraints on lepton asymmetry and radiation energy density: Implications for Planck," JCAP **0806** (2008) 028, arXiv:0804.2971 [astro-ph].

[94] M. Shiraishi, K. Ichikawa, K. Ichiki, N. Sugiyama, and M. Yamaguchi, "Constraints on neutrino masses from WMAP5 and BBN in the lepton asymmetric universe," JCAP **0907** (2009) 005, arXiv:0904.4396 [astro-ph.CO].

[95] A. Caramete and L. A. Popa, "Cosmological evidence for leptonic asymmetry after Planck," JCAP **1402** (2014) 012, arXiv:1311.3856 [astro-ph.CO].

[96] G. Barenboim, W. H. Kinney, and W.-I. Park, "Flavor versus mass eigenstates in neutrino asymmetries: implications for cosmology," arXiv:1609.03200 (2016) , arXiv:1609.03200 [astro-ph.CO].

[97] D. J. Schwarz and M. Stuke, "Does the CMB prefer a leptonic Universe?," New J. Phys. **15** (2013) 033021, arXiv:1211.6721 [astro-ph.CO]. [New J. Phys.15,033021(2013)].

[98] V. Simha and G. Steigman, "Constraining The Universal Lepton Asymmetry," JCAP **0808** (2008) 011, arXiv:0806.0179 [hep-ph].

[99] G. Mangano, G. Miele, S. Pastor, O. Pisanti, and S. Sarikas, "Updated BBN bounds on the cosmological lepton asymmetry for non-zero θ_{13}," Phys. Lett. **B708** (2012) 1–5, arXiv:1110.4335 [hep-ph].

[100] A. D. Dolgov, S. H. Hansen, S. Pastor, S. T. Petcov, G. G. Raffelt, and D. V. Semikoz, "Cosmological bounds on neutrino degeneracy improved by flavor oscillations," Nucl. Phys. **B632** (2002) 363–382, arXiv:hep-ph/0201287 [hep-ph].

[101] Y. Y. Y. Wong, "Analytical treatment of neutrino asymmetry equilibration from flavor oscillations in the early universe," Phys. Rev. **D66** (2002) 025015, arXiv:hep-ph/0203180 [hep-ph].

[102] L. Johns, M. Mina, V. Cirigliano, M. W. Paris, and G. M. Fuller, "Neutrino flavor transformation in the lepton-asymmetric universe," Phys. Rev. **D94** (2016) no. 8, 083505, arXiv:1608.01336 [hep-ph].

[103] G. Barenboim, W. H. Kinney, and W.-I. Park, "Resurrection of large lepton number asymmetries from neutrino flavor oscillations," Phys. Rev. **D95** (2017) no. 4, 043506, arXiv:1609.01584 [hep-ph].

[104] S. Pastor, T. Pinto, and G. G. Raffelt, "Relic density of neutrinos with primordial asymmetries," Phys. Rev. Lett. **102** (2009) 241302, arXiv:0808.3137 [astro-ph].

[105] E. Bulbul, M. Markevitch, A. Foster, R. K. Smith, M. Loewenstein, and S. W. Randall, "Detection of an Unidentified Emission Line in the Stacked X-Ray Spectrum of Galaxy Clusters," The Astrophysical J. **789** (2014) no. 1, 13. http://stacks.iop.org/0004-637X/789/i=1/a=13.

[106] A. Boyarsky, O. Ruchayskiy, D. Iakubovskyi, and J. Franse, "Unidentified Line in X-Ray Spectra of the Andromeda Galaxy and Perseus Galaxy Cluster," Phys. Rev. Lett. **113** (2014) 251301, arXiv:1402.4119 [astro-ph.CO].

[107] R. Murgia, A. Merle, M. Viel, M. Totzauer, and A. Schneider, ""Non-cold" dark matter at small scales: a general approach," arXiv:1704.07838 [astro-ph.CO].

[108] J. F. Cherry and S. Horiuchi, "Closing in on Resonantly Produced Sterile Neutrino Dark Matter," Phys. Rev. **D95** (2017) no. 8, 083015, arXiv:1701.07874 [hep-ph].

[109] A. G. Riess et al., "A 2.4% Determination of the Local Value of the Hubble Constant," Astrophys. J. **826** (2016) no. 1, 56, arXiv:1604.01424 [astro-ph.CO].

[110] F. Beutler, C. Blake, M. Colless, D. H. Jones, L. Staveley-Smith, L. Campbell, Q. Parker, W. Saunders, and F. Watson, "The 6dF Galaxy Survey: Baryon Acoustic Oscillations and the Local Hubble Constant," Mon. Not. Roy. Astron. Soc. **416** (2011) 3017–3032, arXiv:1106.3366 [astro-ph.CO].

[111] **BOSS** Collaboration, L. Anderson et al., "The clustering of galaxies in the SDSS-III Baryon Oscillation Spectroscopic Survey: baryon acoustic oscillations in the Data Releases 10 and 11 Galaxy samples," Mon. Not. Roy. Astron. Soc. **441** (2014) no. 1, 24–62, arXiv:1312.4877 [astro-ph.CO].

[112] A. J. Cuesta et al., "The clustering of galaxies in the SDSS-III Baryon Oscillation Spectroscopic Survey: Baryon Acoustic Oscillations in the correlation function of LOWZ and CMASS galaxies in Data Release 12," Mon. Not. Roy. Astron. Soc. **457** (2016) no. 2, 1770–1785, arXiv:1509.06371 [astro-ph.CO].

[113] A. J. Ross, L. Samushia, C. Howlett, W. J. Percival, A. Burden, and M. Manera, "The clustering of the SDSS DR7 main Galaxy sample ? I. A 4 per cent distance measure at $z = 0.15$," Mon. Not. Roy. Astron. Soc. **449** (2015) no. 1, 835–847, arXiv:1409.3242 [astro-ph.CO].

[114] L. Lancaster, F.-Y. Cyr-Racine, L. Knox, and Z. Pan, "A tale of two modes: Neutrino free-streaming in the early universe," arXiv:1704.06657 [astro-ph.CO].

[115] G. Sigl and G. Raffelt, "General kinetic description of relativistic mixed neutrinos," Nucl. Phys. **B406** (1993) 423–451.